Multibody System Dynamics (2023) 61:43–76
https://doi.org/10.1007/s11044-023-09923-7

RESEARCH

Autonomous unicycle: modeling, dynamics, and control

Xincheng Cao[1] · Dang Cong Bui[1] · Dénes Takács[2,3] · Gábor Orosz[1,4]

Received: 10 January 2023 / Accepted: 19 June 2023 / Published online: 17 July 2023

Abstract
This article focuses on modeling and analyzing the dynamics of an autonomous unicycle. The equations of motion of the nonholonomic multibody system are derived using the Appellian approach, which enables the use of a minimum number of state variables and results in a system of low complexity. The final equations of motion consist of 8 first-order kinematic differential equations and 6 first-order dynamic differential equations. The stability of the open-loop dynamics is investigated and a PD-type controller with 3 input torques is proposed that enables the unicycle to stabilize its upright position and travel along a straight path. The performance of the closed-loop system is demonstrated via numerical simulations.

Keywords Electric unicycle · Nonholonomic dynamics · Appellian approach · Control design

1 Introduction

Agility and maneuverability are highly desired characteristics of mobile robots. One way to achieve this is by making the uncontrolled system unstable and utilizing high-performance controllers to stabilize the desired maneuvers. A unicycle platform may be utilized to achieve such behavior. This paper focuses on building a modeling and analysis framework

✉ G. Orosz
orosz@umich.edu

X. Cao
owencao@umich.edu

D.C. Bui
bdcong@umich.edu

D. Takács
takacs@mm.bme.hu

[1] Department of Mechanical Engineering, University of Michigan, Ann Arbor, MI 48109, USA

[2] Department of Applied Mechanics, Faculty of Mechanical Engineering, Budapest University of Technology and Economics, Budapest, 1111, Hungary

[3] ELKH-BME Dynamics of Machines Research Group, Budapest University of Technology and Economics, Budapest, 1111, Hungary

[4] Department of Civil and Environmental Engineering, University of Michigan, Ann Arbor, MI 48109, USA

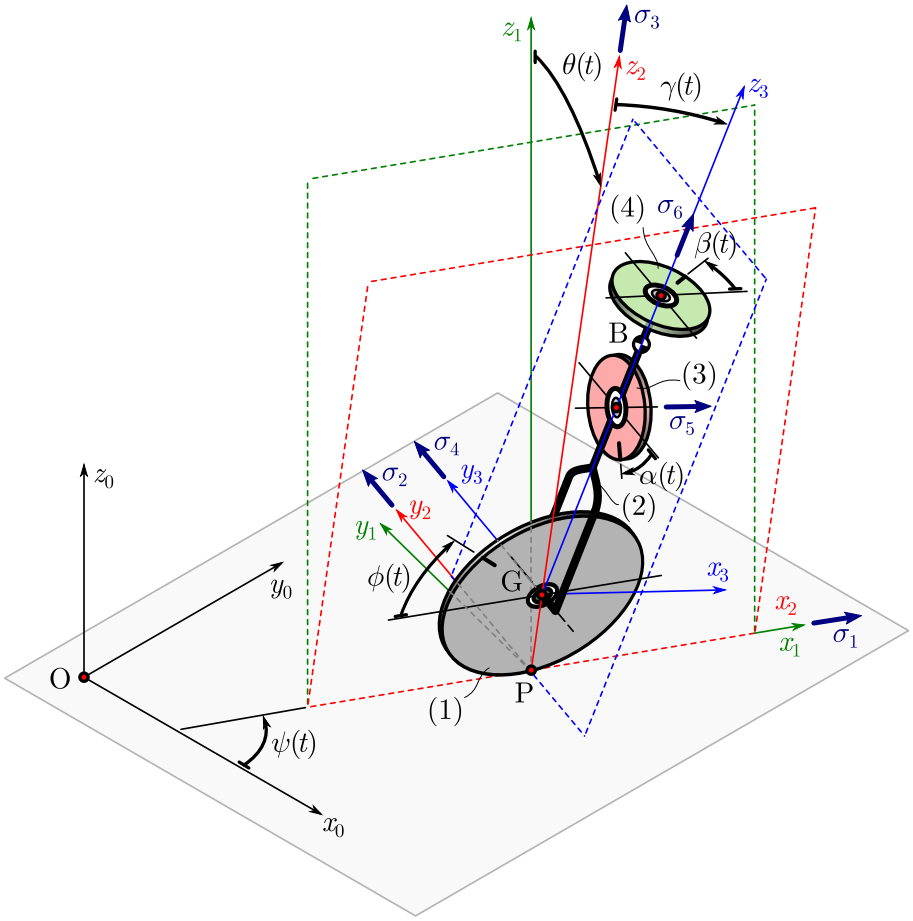

Fig. 1 Mechanical model of the unicycle including the rolling wheel, the body, and two flywheels. The reference frames, the angles, and the angular velocity components are indicated in the figure. (Color figure online)

for the corresponding multibody system consisting of a rolling wheel, a body (to be balanced), and two flywheels used for balancing and maneuvering; see Fig. 1. A feedback design is proposed that enables the unicycle to drive along a straight path while maintaining its upright position. With the rise of human-ridden electric unicycles in our cities we envision autonomous unmanned unicycles to be utilized for freight delivery in urban environments.

While modeling the unicycle we assume a rigid wheel rolling without slipping on the ground, that is, we assume that the single contact point of the wheel has zero velocity. This so-called kinematic constraint results in a so-called nonholonomic system. Nonholonomic systems can be modeled by the Lagrangian approach by introducing Lagrange multipliers (one for each kinematic constraint), where the magnitude of the multipliers represents the magnitude of the constraining forces [29, 39]. However, this leads to differential-algebraic equations that are typically difficult to handle. Instead, in this paper, we utilize the Appellian approach [1, 10], which eliminates the constraining forces and represents the system with a minimum number of state variables. Similar methods were also developed in [13, 16, 37]

and the relationships between different approaches were discussed in [6–8, 17]. More details on nonholonomic systems can be found in [2, 3, 5, 9, 11, 18, 19, 22, 24, 25].

Nonholonomic models have been developed for different classes of mobility devices including automobiles [4, 27, 36], bicycles [14, 20], snake-like robots [12, 40], and even swimming robots [26, 28, 34]. When it comes to unicycles, a few different designs have been studied in the past [33]. For example, in [31] the unicycle was constructed from a rolling wheel, a body, and an overhead flywheel, where the latter represented the twisting torso of a rider. The same setup was utilized in [21, 38] where linear quadratic regulators were proposed to balance the upright position. A different approach was taken in [41], where rather than using an overhead flywheel, a lateral flywheel was considered for balancing. This configuration was utilized in [15, 30] where controllers were also proposed for path tracking. Finally, efforts were also made to model the dynamics of riders for human-powered unicycles in [23, 32] and the latter publication also included experiments with human subjects.

In this paper, for the first time, we investigate an autonomous unmanned unicycle that includes both a balancing flywheel and an overhead flywheel (the latter we refer to as the steering flywheel from now on). By applying the Appellian approach, we select the minimum number of state variables (i.e., generalized coordinates and pseudovelocities) necessary to describe the dynamics. We construct the acceleration energy of the multibody system as a whole, calculate the pseudoforces from the active forces, and derive the equations of motion via the Appell–Gibbs equations. These result in a system of first-order ordinary differential equations. The linearization of the system is used to investigate the stability of the straight running motion analytically and to study the self-stabilizing effects of the speed as a parameter. Then, we utilize a proportional-derivative (PD)-type controller to stabilize the upright position and control the straight running motion of the unicycle. We also demonstrate via numerical simulations in MATLAB that the controller, which is tuned using the linearized system, is able to reject perturbations at the nonlinear level.

This paper is organized as follows. The mechanical model of the unicycle is presented in Sect. 2. The equations of motion are derived in Sect. 3. Stability analysis and control design are performed in Sect. 4, where numerical simulation results are also shown to verify the theoretical findings. Finally, our work is concluded and future research directions are outlined in Sect. 5.

2 Modeling

In this section, we establish the mechanical model of the unicycle, describe the reference frames used, and provide the rolling constraints. The derivation of the governing equations is left for the next section.

2.1 System components and parameters

The mechanical model of the unicycle is shown in Fig. 1. Since the unicycle is autonomous, the construction is simpler than the unicycle models with human riders. The system consists of the following components: a rolling wheel (gray); the body (black); a lateral balancing flywheel (red); a steering flywheel (green). The descriptions of these components are summarized in Table 1.

We apply the following modeling assumptions. (i) The driven wheel is modeled by a rigid disc having a single contact point with the rigid flat ground. Rolling without slipping is considered, namely the velocity of the material point P contacting the ground is zero. The

Table 1 System Parameter Definitions

Parameter	Description
m_{w}	mass of rolling wheel
R	radius of rolling wheel
m	mass of body
h	distance between wheel center point and the center of mass of the body
J_x, J_y, J_z	principal mass moment of inertias of the body
m_{b}	mass of balancing flywheel
r_{b}	radius of balancing flywheel
m_{s}	mass of steering flywheel
r_{s}	radius of steering flywheel

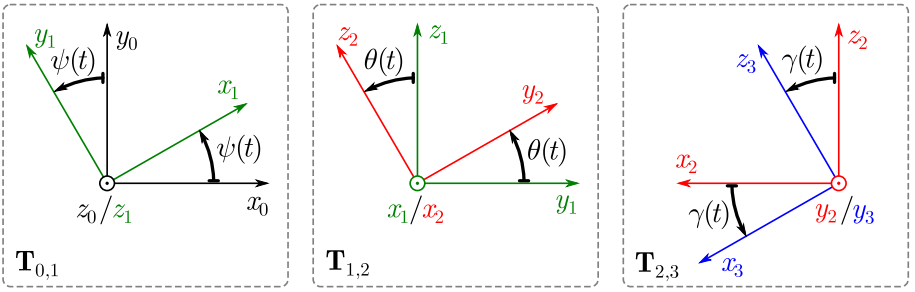

Fig. 2 Definitions of frames with rotations. (Color figure online)

rolling resistance is also ignored, as it does not introduce any significant changes beyond a slight shift in equilibrium pitch angle. (ii) The principal axes of the mass moment of inertia tensor coincide with the symmetry axes of the body. Consequently, the matrix of the inertia tensor is diagonal in the body-fixed frame (when the axis of the frame is aligned with the symmetry axis of the body). (iii) The centers of the lateral balancing and the steering flywheels coincide with the center of mass of body B. (In Fig. 1 these three mass centers are moved apart to increase the readability of the figure). Since the interaction between the body and flywheels is manifested by internal torques, the locations of the flywheels do not influence their effects. These assumptions are introduced to reduce the complexity of the governing equations, while the dynamical behavior of the system remains similar to the behavior of more general configurations.

Finally, the inputs of the system are defined as follows. We apply three electric motors for actuation, hence, an internal driving torque M_{w} is applied between the rolling wheel and the body; the lateral balancing torque M_{b} is applied between the balancing flywheel and the body, and the steering torque M_{s} is applied between the steering flywheel and the body.

2.2 Configurational coordinates and reference frames

To describe the motion of the unicycle, one can introduce multiple reference frames. The ground-fixed frame F_0 is spanned by the x_0, y_0, and z_0 axes; see Figs. 1 and 2. To determine the spatial position of the unicycle in this frame, we use the coordinates x_{G}, y_{G}, and z_{G} of the center of mass G of the rolling wheel. In order to describe the spatial orientation of the

body of the unicycle, we introduce the yaw ψ, tilt θ, and pitch γ angles. Using these, other frames are introduced as explained below.

Frame F_1 is obtained by rotating frame F_0 with the yaw angle ψ about the z_0-axis; see Fig. 2(a). A further rotation of frame F_1 by the tilt angle θ about the x_1-axis leads to frame F_2. Finally, the pitch angle γ is used to rotate frame F_2 about the y_2-axis to obtain the frame F_3. The corresponding frame transformation matrices can be written as follows:

$$\mathbf{T}_{0,1}=\begin{bmatrix} \cos\psi & \sin\psi & 0 \\ -\sin\psi & \cos\psi & 0 \\ 0 & 0 & 1 \end{bmatrix}, \mathbf{T}_{1,2}=\begin{bmatrix} 1 & 0 & 0 \\ 0 & \cos\theta & \sin\theta \\ 0 & -\sin\theta & \cos\theta \end{bmatrix}, \\ \mathbf{T}_{2,3}=\begin{bmatrix} \cos\gamma & 0 & -\sin\gamma \\ 0 & 1 & 0 \\ \sin\gamma & 0 & \cos\gamma \end{bmatrix} \tag{1}$$

and

$$\mathbf{T}_{0,2} = \mathbf{T}_{1,2}\mathbf{T}_{0,1}\,, \qquad \mathbf{T}_{0,3} = \mathbf{T}_{2,3}\mathbf{T}_{1,2}\mathbf{T}_{0,1}\,. \tag{2}$$

These allow us to transform vectors between frames according to

$$\square_{\mathrm{F}_j} = \mathbf{T}_{i,j}\square_{\mathrm{F}_i}\,, \qquad \square_{\mathrm{F}_i} = \mathbf{T}_{i,j}^{\top}\square_{\mathrm{F}_j}\,, \tag{3}$$

where we exploited that $\mathbf{T}_{i,j}$ are orthogonal matrices, i.e., $\mathbf{T}_{i,j}^{-1} = \mathbf{T}_{i,j}^{\top}$.

The angular velocities of the frames (with respect to the ground-fixed frame F_0) can also be derived. For example, the angular velocity of frame F_2 represented in frame F_2 is given by

$$\boldsymbol{\Omega}_2 = \begin{bmatrix} \dot\theta \\ \dot\psi\sin\theta \\ \dot\psi\cos\theta \end{bmatrix}_{\mathrm{F}_2}. \tag{4}$$

Beyond the above-mentioned rotations, three more angles are necessary to determine the rotational positions of the rolling wheel and the two flywheels. The rotation of the rolling wheel about the y_2-axis (relative to frame F_2) is described by the angle ϕ. Similarly, angles α and β characterize the rotations of the balancing flywheel and the steering flywheel about the x_3- and z_3-axis, respectively (relative to the frame F_3).

Thus, without considering the kinematic constraint of rolling, one may use the nine scalar variables $x_G, y_G, z_G, \psi, \theta, \phi, \gamma, \alpha, \beta$ as configurational coordinates.

2.3 Kinematic constraints of rolling

The velocity of the wheel-ground contact point P of the rolling wheel can be derived using the transport formula

$$\mathbf{v}_P = \mathbf{v}_G + \boldsymbol{\omega}_w \times \mathbf{r}_{GP}. \tag{5}$$

The velocity of the center of mass G of the wheel in the F_0 frame is given by

$$\mathbf{v}_G = \begin{bmatrix} \dot x_G \\ \dot y_G \\ \dot z_G \end{bmatrix}_{\mathrm{F}_0}. \tag{6}$$

The angular velocity of the rolling wheel can be resolved in the F_2 frame as

$$\boldsymbol{\omega}_{\mathrm{w}} = \begin{bmatrix} \dot{\theta} \\ \dot{\phi} + \dot{\psi}\sin\theta \\ \dot{\psi}\cos\theta \end{bmatrix}_{\mathrm{F}_2}, \tag{7}$$

and the position vector in the F_2 frame becomes

$$\mathbf{r}_{\mathrm{GP}} = \begin{bmatrix} 0 \\ 0 \\ -R \end{bmatrix}_{\mathrm{F}_2}. \tag{8}$$

By transforming the cross product in (5) from the F_2 frame to the F_0 frame with the help of the matrix $\mathbf{T}_{0,2}^{\top}$ (cf. (1)–(3)) and assuming rolling without slipping, that is,

$$\mathbf{v}_{\mathrm{P}} = \mathbf{0}, \tag{9}$$

one may obtain the constraint equations

$$\begin{cases} \dot{x}_{\mathrm{G}} - \dot{\phi}R\cos\psi - \dot{\psi}R\cos\psi\sin\theta - \dot{\theta}R\sin\psi\cos\theta = 0, & (10) \\ \dot{y}_{\mathrm{G}} - \dot{\phi}R\sin\psi - \dot{\psi}R\sin\psi\sin\theta + \dot{\theta}R\cos\psi\cos\theta = 0, & (11) \\ \dot{z}_{\mathrm{G}} + R\dot{\theta}\sin\theta = 0. & (12) \end{cases}$$

Here, (10) and (11) are so-called nonintegrable kinematic constraints and they will be utilized in the above differential form in the remaining part of this study. On the other hand, (12) can be integrated with respect to time and rephrased as a geometric constraint:

$$z_{\mathrm{G}} = R\cos\theta. \tag{13}$$

As a consequence, the vertical position z_{G} of point G will not be used as a generalized coordinate. That is, the eight generalized coordinates $x_{\mathrm{G}}, y_{\mathrm{G}}, \psi, \theta, \phi, \gamma, \alpha, \beta$ describe the mechanical system unambiguously.

3 Governing equations

The equations of motion of the unicycle are derived here using the Appellian approach [1, 5, 9, 10]. To obtain more details about the approach, the role of the pseudovelocities, and their appropriate choice, we refer the reader to [27], as an entry point to the literature. After choosing the pseudovelocities we construct the acceleration energy of the system which is used to derive the left-hand side of the Appell–Gibbs equations. The pseudoforces, which show up on the right-hand sides of the equations, are obtained by calculating the virtual power of the active forces and torques.

3.1 Pseudovelocities

The angular velocity of the body can be resolved in the F_2 frame as

$$\boldsymbol{\omega} = \begin{bmatrix} \dot{\theta} \\ \dot{\gamma} + \dot{\psi}\sin\theta \\ \dot{\psi}\cos\theta \end{bmatrix}_{\mathrm{F}_2}, \tag{14}$$

cf. (7). One may transform this to the F_3 frame using the transformation matrix $\mathbf{T}_{2,3}$ (cf. (1)–(3)):

$$\boldsymbol{\omega} = \begin{bmatrix} \dot{\theta}\cos\gamma - \dot{\psi}\cos\theta\sin\gamma \\ \dot{\gamma} + \dot{\psi}\sin\theta \\ \dot{\theta}\sin\gamma + \dot{\psi}\cos\theta\cos\gamma \end{bmatrix}_{F_3} . \tag{15}$$

Similarly, the angular velocities of the balancing flywheel and the steering flywheel can be derived as

$$\boldsymbol{\omega}_b = \begin{bmatrix} \dot{\alpha} + \dot{\theta}\cos\gamma - \dot{\psi}\cos\theta\sin\gamma \\ \dot{\gamma} + \dot{\psi}\sin\theta \\ \dot{\theta}\sin\gamma + \dot{\psi}\cos\theta\cos\gamma \end{bmatrix}_{F_3} , \quad \boldsymbol{\omega}_s = \begin{bmatrix} \dot{\theta}\cos\gamma - \dot{\psi}\cos\theta\sin\gamma \\ \dot{\gamma} + \dot{\psi}\sin\theta \\ \dot{\beta} + \dot{\theta}\sin\gamma + \dot{\psi}\cos\theta\cos\gamma \end{bmatrix}_{F_3} . \tag{16}$$

Since the system has eight generalized coordinates and two kinematic constraints, six pseudovelocities are required to accomplish the derivation of governing equations and they can be defined as follows. The components of the angular velocity $\boldsymbol{\omega}_w$ of the wheel (see (7)) are used to define the pseudovelocities σ_1, σ_2, and σ_3, respectively. The second component of the angular velocity $\boldsymbol{\omega}$ of the body, the first component of the angular velocity $\boldsymbol{\omega}_b$ of the balancing flywheel, and the third component of the angular velocity $\boldsymbol{\omega}_s$ of the steering flywheel are used as σ_4, σ_5, and σ_6, respectively. That is, the pseudovelocities are as follows:

$$\begin{aligned} \sigma_1 &:= \dot{\theta} , \\ \sigma_2 &:= \dot{\phi} + \dot{\psi}\sin\theta , \\ \sigma_3 &:= \dot{\psi}\cos\theta , \\ \sigma_4 &:= \dot{\gamma} + \dot{\psi}\sin\theta , \\ \sigma_5 &:= \dot{\alpha} + \dot{\theta}\cos\gamma - \dot{\psi}\cos\theta\sin\gamma , \\ \sigma_6 &:= \dot{\beta} + \dot{\theta}\sin\gamma + \dot{\psi}\cos\theta\cos\gamma . \end{aligned} \tag{17}$$

These definitions together with the kinematic constraints (10) and (11) lead to the linear system

$$\begin{bmatrix} 1 & 0 & -R\cos\psi\sin\theta & -R\sin\psi\cos\theta & -R\cos\psi & 0 & 0 & 0 \\ 0 & 1 & -R\sin\psi\sin\theta & R\cos\psi\cos\theta & -R\sin\psi & 0 & 0 & 0 \\ 0 & 0 & 0 & 1 & 0 & 0 & 0 & 0 \\ 0 & 0 & \sin\theta & 0 & 1 & 0 & 0 & 0 \\ 0 & 0 & \cos\theta & 0 & 0 & 0 & 0 & 0 \\ 0 & 0 & \sin\theta & 0 & 0 & 1 & 0 & 0 \\ 0 & 0 & -\cos\theta\sin\gamma & \cos\gamma & 0 & 0 & 1 & 0 \\ 0 & 0 & \cos\theta\cos\gamma & \sin\gamma & 0 & 0 & 0 & 1 \end{bmatrix} \begin{bmatrix} \dot{x}_G \\ \dot{y}_G \\ \dot{\psi} \\ \dot{\theta} \\ \dot{\phi} \\ \dot{\gamma} \\ \dot{\alpha} \\ \dot{\beta} \end{bmatrix} = \begin{bmatrix} 0 \\ 0 \\ \sigma_1 \\ \sigma_2 \\ \sigma_3 \\ \sigma_4 \\ \sigma_5 \\ \sigma_6 \end{bmatrix} . \tag{18}$$

The determinant of the square matrix above is $\cos\theta$, that is, the matrix is only singular for $\theta = \pm\pi/2$, which corresponds to the wheel lying on the ground. This indicates that the selection of pseudovelocities is appropriate. Solving (18) provides the generalized velocities

expressed as functions of the pseudovelocities and generalized coordinates:

$$\begin{aligned}
\dot{\theta} &= \sigma_1 \,, \\
\dot{\gamma} &= \sigma_4 - \sigma_3 \tan\theta \,, \\
\dot{\psi} &= \frac{\sigma_3}{\cos\theta} \,, \\
\dot{x}_{\mathrm{G}} &= \sigma_2 R \cos\psi + \sigma_1 R \sin\psi \cos\theta \,, \\
\dot{y}_{\mathrm{G}} &= \sigma_2 R \sin\psi - \sigma_1 R \cos\psi \cos\theta \,, \\
\dot{\phi} &= \sigma_2 - \sigma_3 \tan\theta \,, \\
\dot{\alpha} &= \sigma_5 - \sigma_1 \cos\gamma + \sigma_3 \sin\gamma \,, \\
\dot{\beta} &= \sigma_6 - \sigma_1 \sin\gamma - \sigma_3 \cos\gamma \,.
\end{aligned} \tag{19}$$

Here, the equations are ordered while considering the linearization performed further below. We remark that the choice of pseudovelocities is not unique. For example, one may choose the angular-velocity components of the bodies in other frames. The choice made here was found to provide equations of lower complexity while retaining a clear physical meaning for each pseudovelocity.

3.2 Acceleration energy

The total acceleration energy S of the unicycle can be obtained by combining the acceleration energies of the four rigid bodies:

$$S = S_{\mathrm{wheel}} + S_{\mathrm{body}} + S_{\mathrm{balance}} + S_{\mathrm{steer}} \,, \tag{20}$$

where S_{wheel}, S_{body}, S_{balance}, and S_{steer} are the acceleration energies of the rolling wheel, the body, the balancing flywheel, and the steering flywheel, respectively. The following subsections will present the calculations of each acceleration energy component.

3.2.1 Rolling wheel

It is convenient to calculate the acceleration energy of the rolling wheel in frame F_2. The mass moment of inertia tensor at the center of mass G is

$$\mathbf{J}_{\mathrm{w}} = \frac{m_{\mathrm{w}} R^2}{4} \begin{bmatrix} 1 & 0 & 0 \\ 0 & 2 & 0 \\ 0 & 0 & 1 \end{bmatrix}_{\mathrm{F}_2} . \tag{21}$$

Using the definitions (17) of the pseudovelocities, the angular velocity (7) of the rolling wheel can be represented as

$$\boldsymbol{\omega}_{\mathrm{w}} = \begin{bmatrix} \sigma_1 \\ \sigma_2 \\ \sigma_3 \end{bmatrix}_{\mathrm{F}_2} . \tag{22}$$

Similarly, the angular velocity (4) of frame F_2 can be written as

$$\mathbf{\Omega}_2 = \begin{bmatrix} \sigma_1 \\ \sigma_3 \tan\theta \\ \sigma_3 \end{bmatrix}_{F_2}. \tag{23}$$

Finally, using (5), (8), (9), and (22) the velocity of the center of mass G of the rolling wheel can be formulated as

$$\mathbf{v}_G = \begin{bmatrix} \sigma_2 R \\ -\sigma_1 R \\ 0 \end{bmatrix}_{F_2}. \tag{24}$$

The time derivatives of the velocity (24) and the angular velocity (22) can be calculated via the frame derivatives. Hence, the acceleration of the center of mass G and the angular acceleration of the rolling wheel can be derived:

$$\mathbf{a}_G = \dot{\mathbf{v}}_G = \begin{bmatrix} R(\dot{\sigma}_2 + \sigma_1\sigma_3) \\ -R(\dot{\sigma}_1 - \sigma_2\sigma_3) \\ -R\left(\sigma_1^2 + \sigma_2\sigma_3\tan\theta\right) \end{bmatrix}_{F_2}, \quad \boldsymbol{\alpha}_w = \dot{\boldsymbol{\omega}}_w = \begin{bmatrix} \dot{\sigma}_1 - \sigma_2\sigma_3 + \sigma_3^2\tan\theta \\ \dot{\sigma}_2 \\ \dot{\sigma}_3 + \sigma_1\sigma_2 - \sigma_1\sigma_3\tan\theta \end{bmatrix}_{F_2}, \tag{25}$$

where the dots above the vectors represent the time derivative in the ground-fixed frame F_0.

Then, the acceleration energy of the rolling wheel can be constructed as

$$\begin{aligned} S_{\text{wheel}} &= \frac{1}{2} m_w \mathbf{a}_G^2 + \frac{1}{2}\boldsymbol{\alpha}_w \cdot \mathbf{J}_w\boldsymbol{\alpha}_w + \boldsymbol{\alpha}_w \cdot (\boldsymbol{\omega}_w \times \mathbf{J}_w\boldsymbol{\omega}_w) + \cdots \\ &= m_w R^2 \left(\frac{5}{8}\dot{\sigma}_1^2 + \frac{{\sigma_3}^2\tan\theta - 6\sigma_2\sigma_3}{4}\dot{\sigma}_1 + \frac{3}{4}\dot{\sigma}_2^2 + \sigma_1\sigma_3\dot{\sigma}_2 \right. \\ &\quad \left. + \frac{1}{8}\dot{\sigma}_3^2 + \frac{2\sigma_1\sigma_2 - \sigma_1\sigma_3\tan\theta}{4}\dot{\sigma}_3 \right) + \cdots, \end{aligned} \tag{26}$$

where $\cdot$ between vectors denotes the dot product, while $\cdots$ refer to terms that do not depend on the pseudoaccelerations. These terms are not spelled out since they will not play any role when deriving the Appell equations.

3.2.2 Body

The mass moment of inertia tensor of the body at the center of mass B can be represented in the F_3 frame as

$$\mathbf{J} = \begin{bmatrix} J_x & 0 & 0 \\ 0 & J_y & 0 \\ 0 & 0 & J_z \end{bmatrix}_{F_3}. \tag{27}$$

Using the definitions of the pseudovelocities (17), the angular velocity (15) of the body can be expressed in the F_3 frame as

$$\boldsymbol{\omega} = \begin{bmatrix} \sigma_1\cos\gamma - \sigma_3\sin\gamma \\ \sigma_4 \\ \sigma_1\sin\gamma + \sigma_3\cos\gamma \end{bmatrix}_{F_3}. \tag{28}$$

Note that this also gives the angular velocity of the frame F_3, which is attached to the body. One may also transform the velocity (24) of the center of mass G of the wheel to the F_3 frame using the matrix $\mathbf{T}_{2,3}$ (cf. (1)–(3)):

$$\mathbf{v}_{\mathrm{G}} = \begin{bmatrix} \sigma_2 R\cos\gamma \\ -\sigma_1 R \\ \sigma_2 R\sin\gamma \end{bmatrix}_{\mathrm{F}_3}, \tag{29}$$

and we have the position vector

$$\mathbf{r}_{\mathrm{GB}} = \begin{bmatrix} 0 \\ 0 \\ h \end{bmatrix}_{\mathrm{F}_3}. \tag{30}$$

Thus, the velocity of the center of mass B of the body can be calculated as

$$\mathbf{v}_{\mathrm{B}} = \mathbf{v}_{\mathrm{G}} + \boldsymbol{\omega}\times\mathbf{r}_{\mathrm{GB}} = \begin{bmatrix} \sigma_2 R\cos\gamma + \sigma_4 h \\ -\sigma_1(R + h\cos\gamma) + \sigma_3 h\sin\gamma \\ \sigma_2 R\sin\gamma \end{bmatrix}_{\mathrm{F}_3}. \tag{31}$$

The acceleration of the center of mass B and the angular acceleration can be obtained using frame derivatives:

$$\mathbf{a}_{\mathrm{B}} = \dot{\mathbf{v}}_{\mathrm{B}} = \begin{bmatrix} a_{\mathrm{B}x} \\ a_{\mathrm{B}y} \\ a_{\mathrm{B}z} \end{bmatrix}_{\mathrm{F}_3}, \quad \boldsymbol{\alpha} = \dot{\boldsymbol{\omega}} = \begin{bmatrix} \alpha_x \\ \alpha_y \\ \alpha_z \end{bmatrix}_{\mathrm{F}_3}, \tag{32}$$

and the detailed expressions are given by (A1) and (A2) in Appendix A.

Thus, the acceleration energy of the body can be calculated as

$$\begin{aligned} S_{\mathrm{body}} =& \frac{1}{2}m\mathbf{a}_{\mathrm{B}}^2 + \frac{1}{2}\boldsymbol{\alpha}\cdot\mathbf{J}\boldsymbol{\alpha} + \boldsymbol{\alpha}\cdot(\boldsymbol{\omega}\times\mathbf{J}\boldsymbol{\omega}) + \cdots \\ =& \frac{1}{2}\Big(mR^2 + \big(J_x + mh^2\big)\cos^2\gamma + J_z\sin^2\gamma + 2mRh\cos\gamma\Big)\dot{\sigma}_1^2 \\ &+ \Big(\sigma_3^2\Big(\big(J_x + mh^2\big)\cos^2\gamma + J_z\sin^2\gamma + mRh\cos\gamma\Big)\tan\theta \\ &\quad + \sigma_1\sigma_3\Big(\big(J_x + mh^2 - J_z\big)\cos\gamma + mRh\Big)\tan\theta\sin\gamma \\ &\quad - 2\sigma_1\sigma_4\Big(\big(J_x + mh^2 - J_z\big)\cos\gamma + mRh\Big)\sin\gamma \\ &\quad - \sigma_2\sigma_3\Big(mR^2 + mRh\cos\gamma\Big) \\ &\quad + \sigma_3\sigma_4\Big(J_x - J_y + J_z\big(\cos^2\gamma - \sin^2\gamma\big) - 2\big(J_x + mh^2\big)\cos^2\gamma \\ &\qquad\qquad - 2mRh\cos\gamma\Big)\Big)\dot{\sigma}_1 \\ &+ \frac{1}{2}mR^2\dot{\sigma}_2^2 + \Big(-\big(\sigma_3^2 + \sigma_4^2\big)mRh\sin\gamma + \sigma_1\sigma_3\big(mR^2 + mRh\cos\gamma\big)\Big)\dot{\sigma}_2 \end{aligned}$$

$$
\begin{aligned}
&+\frac{1}{2}\Big(\big(J_x+mh^2\big)\sin^2\gamma+J_z\cos^2\gamma\Big)\dot{\sigma}_3^2\\
&+\Big(-\sigma_3^2\Big(J_x+mh^2-J_z\Big)\tan\theta\cos\gamma\sin\gamma\\
&\quad-\sigma_1\sigma_3\Big(\big(J_x+mh^2\big)\sin^2\gamma+J_z\cos^2\gamma\Big)\tan\theta\\
&\quad+\sigma_1\sigma_4\Big(-J_x+J_y+J_z\big(\cos^2\gamma-\sin^2\gamma\big)+2\big(J_x+mh^2\big)\sin^2\gamma\Big)\\
&\quad+\sigma_2\sigma_3 mRh\sin\gamma+2\sigma_3\sigma_4\Big(J_x+mh^2-J_z\Big)\cos\gamma\sin\gamma\Big)\dot{\sigma}_3\\
&+\frac{1}{2}\big(J_y+mh^2\big)\dot{\sigma}_4^2\\
&+\Big(\sigma_1^2\Big(\big(J_x+mh^2-J_z\big)\cos\gamma+mRh\Big)\sin\gamma\\
&\quad-\sigma_3^2\Big(J_x+mh^2-J_z\Big)\cos\gamma\sin\gamma\\
&\quad+\sigma_1\sigma_3\Big(\big(J_x+mh^2-J_z\big)\big(\cos^2\gamma-\sin^2\gamma\big)+mRh\cos\gamma\Big)\\
&\quad+\sigma_2\sigma_3 mRh\tan\theta\sin\gamma\Big)\dot{\sigma}_4\\
&-\Big(\big(J_x+mh^2-J_z\big)\cos\gamma+mRh\Big)\sin\gamma\,\dot{\sigma}_1\dot{\sigma}_3+mRh\cos\gamma\,\dot{\sigma}_2\dot{\sigma}_4+\cdots. \qquad (33)
\end{aligned}
$$

3.2.3 Flywheels

The mass moment of inertia tensors at the centers of masses of the flywheels are

$$
\mathbf{J}_{\mathrm{b}}=\frac{m_{\mathrm{b}}r_{\mathrm{b}}^2}{4}\begin{bmatrix}2&0&0\\0&1&0\\0&0&1\end{bmatrix}_{\mathrm{F}_3},\quad \mathbf{J}_{\mathrm{s}}=\frac{m_{\mathrm{s}}r_{\mathrm{s}}^2}{4}\begin{bmatrix}1&0&0\\0&1&0\\0&0&2\end{bmatrix}_{\mathrm{F}_3}. \qquad (34)
$$

Since the centers of masses of both flywheels coincide with that of the body, their accelerations are equal to $\mathbf{a}_{\mathrm{B}}$ in (32). The angular velocities of flywheels can be obtained by substituting the definitions of the pseudovelocities (17) into (16):

$$
\boldsymbol{\omega}_{\mathrm{b}}=\begin{bmatrix}\sigma_5\\ \sigma_4\\ \sigma_1\sin\gamma+\sigma_3\cos\gamma\end{bmatrix}_{\mathrm{F}_3},\quad \boldsymbol{\omega}_{\mathrm{s}}=\begin{bmatrix}\sigma_1\cos\gamma-\sigma_3\sin\gamma\\ \sigma_4\\ \sigma_6\end{bmatrix}_{\mathrm{F}_3}. \qquad (35)
$$

Similarly to the previous sections, the angular accelerations of the flywheels can be calculated using frame derivatives:

$$
\boldsymbol{\alpha}_{\mathrm{b}}=\begin{bmatrix}\alpha_{\mathrm{b}x}\\ \alpha_{\mathrm{b}y}\\ \alpha_{\mathrm{b}z}\end{bmatrix}_{\mathrm{F}_3},\quad \boldsymbol{\alpha}_{\mathrm{s}}=\begin{bmatrix}\alpha_{\mathrm{s}x}\\ \alpha_{\mathrm{s}y}\\ \alpha_{\mathrm{s}z}\end{bmatrix}_{\mathrm{F}_3}, \qquad (36)
$$

and the detailed expressions are given by (A3) and (A4) in Appendix A. Hence, the acceleration energies of the flywheels are:

$$
\begin{aligned}
S_{\text{balance}} =& \frac{1}{2} m_{\text{b}} \mathbf{a}_{\text{B}}^2 + \frac{1}{2} \boldsymbol{\alpha}_{\text{b}} \cdot \mathbf{J}_{\text{b}} \boldsymbol{\alpha}_{\text{b}} + \boldsymbol{\alpha}_{\text{b}} \cdot (\boldsymbol{\omega}_{\text{b}} \times \mathbf{J}_{\text{b}} \boldsymbol{\omega}_{\text{b}}) + \cdots \\
=& \frac{1}{2} m_{\text{b}} \Big(\big(R + h\cos\gamma\big)^2 + \frac{r_{\text{b}}^2}{4} \sin^2\gamma \Big) \dot{\sigma}_1^2 \\
&+ m_{\text{b}} \Big(\sigma_3^2 \Big(h^2 \cos^2\gamma + \frac{r_{\text{b}}^2}{4} \sin^2\gamma + Rh\cos\gamma \Big) \tan\theta \\
&\qquad + \sigma_1\sigma_3 \Big(\big(h^2 - \frac{r_{\text{b}}^2}{4}\big) \cos\gamma + Rh \Big) \tan\theta \sin\gamma \\
&\qquad - 2\sigma_1\sigma_4 \Big(\big(h^2 - \frac{r_{\text{b}}^2}{4}\big) \cos\gamma + Rh \Big) \sin\gamma \\
&\qquad - \sigma_2\sigma_3 \big(R^2 + Rh\cos\gamma \big) \\
&\qquad - 2\sigma_3\sigma_4 \Big(h^2 \cos^2\gamma + \frac{r_{\text{b}}^2}{4} \sin^2\gamma + Rh\cos\gamma \Big) \\
&\qquad - \frac{1}{2} \sigma_4\sigma_5 r_{\text{b}}^2 \sin\gamma \Big) \dot{\sigma}_1 \\
&+ \frac{1}{2} m_{\text{b}} R^2 \dot{\sigma}_2^2 - m_{\text{b}} \Big(\big(\sigma_3^2 + \sigma_4^2\big) Rh \sin\gamma - \sigma_1\sigma_3 \big(R^2 + Rh\cos\gamma \big) \Big) \dot{\sigma}_2 \\
&+ \frac{1}{2} m_{\text{b}} \Big(h^2 \sin^2\gamma + \frac{r_{\text{b}}^2}{4} \cos^2\gamma \Big) \dot{\sigma}_3^2 \\
&+ m_{\text{b}} \Big(- \sigma_3^2 \Big(h^2 - \frac{r_{\text{b}}^2}{4} \Big) \tan\theta \cos\gamma \sin\gamma \\
&\qquad - \sigma_1\sigma_3 \Big(h^2 \sin^2\gamma + \frac{r_{\text{b}}^2}{4} \cos^2\gamma \Big) \tan\theta \\
&\qquad + 2\sigma_1\sigma_4 \Big(h^2 \sin^2\gamma + \frac{r_{\text{b}}^2}{4} \cos^2\gamma \Big) + \sigma_2\sigma_3 Rh \sin\gamma \\
&\qquad + 2\sigma_3\sigma_4 \Big(h^2 - \frac{r_{\text{b}}^2}{4} \Big) \cos\gamma \sin\gamma - \frac{1}{2} \sigma_4\sigma_5 r_{\text{b}}^2 \cos\gamma \Big) \dot{\sigma}_3 \\
&+ \frac{1}{2} m_{\text{b}} \Big(h^2 + \frac{r_{\text{b}}^2}{4} \Big) \dot{\sigma}_4^2 \\
&+ m_{\text{b}} \Big(\sigma_1^2 \Big(\big(h^2 - \frac{r_{\text{b}}^2}{4}\big) \cos\gamma + Rh \Big) \sin\gamma \\
&\qquad - \sigma_3^2 \Big(h^2 - \frac{r_{\text{b}}^2}{4} \Big) \cos\gamma \sin\gamma \\
&\qquad + \sigma_1\sigma_3 \Big(\big(h^2 - \frac{r_{\text{b}}^2}{4}\big) \big(\cos^2\gamma - \sin^2\gamma \big) + Rh\cos\gamma \Big) \\
&\qquad + \frac{1}{2} \sigma_1\sigma_5 r_{\text{b}}^2 \sin\gamma + \sigma_2\sigma_3 Rh \tan\theta \sin\gamma + \frac{1}{2} \sigma_3\sigma_5 r_{\text{b}}^2 \cos\gamma \Big) \dot{\sigma}_4
\end{aligned}
$$

$$+\frac{1}{4}m_{\mathrm{b}}r_{\mathrm{b}}^2\,\dot{\sigma}_5^2$$
$$-m_{\mathrm{b}}\Big(\Big(h^2-\frac{r_{\mathrm{b}}^2}{4}\Big)\cos\gamma+Rh\Big)\sin\gamma\,\dot{\sigma}_1\dot{\sigma}_3+m_{\mathrm{b}}Rh\cos\gamma\,\dot{\sigma}_2\dot{\sigma}_4+\cdots \tag{37}$$

and

$$\begin{aligned}
S_{\mathrm{steer}} =& \frac{1}{2}m_{\mathrm{s}}\mathbf{a}_{\mathrm{B}}^2+\frac{1}{2}\boldsymbol{\alpha}_{\mathrm{s}}\cdot\mathbf{J}_{\mathrm{s}}\boldsymbol{\alpha}_{\mathrm{s}}+\boldsymbol{\alpha}_{\mathrm{s}}\cdot(\boldsymbol{\omega}_{\mathrm{s}}\times\mathbf{J}_{\mathrm{s}}\boldsymbol{\omega}_{\mathrm{s}})+\cdots\\
=&\frac{1}{2}m_{\mathrm{s}}\Big(\big(R+h\cos\gamma\big)^2+\frac{r_{\mathrm{s}}^2}{4}\cos^2\gamma\Big)\dot{\sigma}_1^2\\
&+m_{\mathrm{s}}\Big(\sigma_3^2\Big(h^2\cos^2\gamma+\frac{r_{\mathrm{s}}^2}{4}\cos^2\gamma+Rh\cos\gamma\Big)\tan\theta\\
&\qquad+\sigma_1\sigma_3\Big(\big(h^2+\frac{r_{\mathrm{s}}^2}{4}\big)\cos\gamma+Rh\Big)\tan\theta\sin\gamma\\
&\qquad-2\sigma_1\sigma_4\Big(\big(h^2+\frac{r_{\mathrm{s}}^2}{4}\big)\cos\gamma+Rh\Big)\sin\gamma\\
&\qquad-\sigma_2\sigma_3\big(R^2+Rh\cos\gamma\big)\\
&\qquad-2\sigma_3\sigma_4\Big(h^2\cos^2\gamma+\frac{r_{\mathrm{s}}^2}{4}\cos^2\gamma+Rh\cos\gamma\Big)\\
&\qquad+\frac{1}{2}\sigma_4\sigma_6r_{\mathrm{s}}^2\cos\gamma\Big)\dot{\sigma}_1\\
&+\frac{1}{2}m_{\mathrm{s}}R^2\dot{\sigma}_2^2-m_{\mathrm{s}}\Big(\big(\sigma_3^2+\sigma_4^2\big)Rh\sin\gamma-\sigma_1\sigma_3\big(R^2+Rh\cos\gamma\big)\Big)\dot{\sigma}_2\\
&+\frac{1}{2}m_{\mathrm{s}}\Big(h^2+\frac{r_{\mathrm{s}}^2}{4}\Big)\sin^2\gamma\,\dot{\sigma}_3^2\\
&+m_{\mathrm{s}}\Big(-\sigma_3^2\Big(h^2+\frac{r_{\mathrm{s}}^2}{4}\Big)\tan\theta\cos\gamma\sin\gamma\\
&\qquad-\sigma_1\sigma_3\Big(\big(h^2+\frac{r_{\mathrm{s}}^2}{4}\big)\sin^2\gamma\Big)\tan\theta\\
&\qquad+2\sigma_1\sigma_4\Big(\big(h^2+\frac{r_{\mathrm{s}}^2}{4}\big)\sin^2\gamma\Big)+\sigma_2\sigma_3Rh\sin\gamma\\
&\qquad+2\sigma_3\sigma_4\Big(h^2+\frac{r_{\mathrm{s}}^2}{4}\Big)\cos\gamma\sin\gamma-\frac{1}{2}\sigma_4\sigma_6r_{\mathrm{s}}^2\sin\gamma\Big)\dot{\sigma}_3\\
&+\frac{1}{2}m_{\mathrm{s}}\Big(h^2+\frac{r_{\mathrm{s}}^2}{4}\Big)\dot{\sigma}_4^2\\
&+m_{\mathrm{s}}\Big(\sigma_1^2\Big(\big(h^2+\frac{r_{\mathrm{s}}^2}{4}\big)\cos\gamma+Rh\Big)\sin\gamma\\
&\qquad-\sigma_3^2\Big(h^2+\frac{r_{\mathrm{s}}^2}{4}\Big)\cos\gamma\sin\gamma
\end{aligned}$$

$$+\sigma_1\sigma_3\Big(\big(h^2+\frac{r_s^2}{4}\big)\big(\cos^2\gamma-\sin^2\gamma\big)+Rh\cos\gamma\Big)$$
$$-\frac{1}{2}\sigma_1\sigma_6 r_s^2\cos\gamma+\sigma_2\sigma_3 Rh\tan\theta\sin\gamma+\frac{1}{2}\sigma_3\sigma_6 r_s^2\sin\gamma\Big)\dot{\sigma}_4$$
$$+\frac{1}{4}m_s r_s^2\dot{\sigma}_6^2$$
$$-m_s\left(\left(h^2+\frac{r_s^2}{4}\right)\cos\gamma+Rh\right)\sin\gamma\,\dot{\sigma}_1\dot{\sigma}_3+m_s Rh\cos\gamma\,\dot{\sigma}_2\dot{\sigma}_4+\cdots. \tag{38}$$

3.3 Virtual power and pseudoforces

To determine the pseudoforces, which give the right-hand sides of the Appell equations, the virtual power of the active forces is required.

For the rolling wheel, the gravitational force points to the negative z_0 direction in the F_0 frame. To transform this to the F_2 frame one may use the rotation matrix $\mathbf{T}_{0,2}$ (cf. (1)–(3)):

$$\mathbf{G}_w=\begin{bmatrix}0\\-m_w g\sin\theta\\-m_w g\cos\theta\end{bmatrix}_{F_2}. \tag{39}$$

The driving torque applied at the rolling wheel can be written as

$$\mathbf{M}_w=\begin{bmatrix}0\\M_w\\0\end{bmatrix}_{F_2}. \tag{40}$$

These, together with $\boldsymbol{\omega}_w$ in (22) and $\mathbf{v}_G$ in (24), allow the calculation of the virtual power

$$\begin{aligned}\delta P_{\text{wheel}}&=\mathbf{G}_w\cdot\delta\mathbf{v}_G+\mathbf{M}_w\cdot\delta\boldsymbol{\omega}_w\\&=m_w g R\sin\theta\,\delta\sigma_1+M_w\,\delta\sigma_2,\end{aligned} \tag{41}$$

where δ refers to virtual quantities.

The virtual power of the forces acting on the lateral balancing and steering flywheels can be derived in a similar manner. The gravitational forces acting on the flywheels also point in the negative z_0 direction in the F_0 frame and they can be transformed to the F_3 frame using the rotation matrix $\mathbf{T}_{0,3}$ (cf. (1)–(3)):

$$\mathbf{G}_b=\begin{bmatrix}m_b g\cos\theta\sin\gamma\\-m_b g\sin\theta\\-m_b g\cos\theta\cos\gamma\end{bmatrix}_{F_3},\quad \mathbf{G}_s=\begin{bmatrix}m_s g\cos\theta\sin\gamma\\-m_s g\sin\theta\\-m_s g\cos\theta\cos\gamma\end{bmatrix}_{F_3}, \tag{42}$$

while the balancing and steering torques are given by

$$\mathbf{M}_b=\begin{bmatrix}M_b\\0\\0\end{bmatrix}_{F_3},\quad \mathbf{M}_s=\begin{bmatrix}0\\0\\M_s\end{bmatrix}_{F_3}, \tag{43}$$

respectively.

Using $\boldsymbol{\omega}_\mathrm{b}$ and $\boldsymbol{\omega}_\mathrm{s}$ in (35), as well as $\mathbf{v}_\mathrm{B}$ in (31), the virtual powers of the forces acting on the flywheels can be written as

$$\begin{aligned}\delta P_{\text{balance}} =& \mathbf{G}_\mathrm{b} \cdot \delta \mathbf{v}_\mathrm{B} + \mathbf{M}_\mathrm{b} \cdot \delta \boldsymbol{\omega}_\mathrm{b} \\ =& \big(m_\mathrm{b} g R \sin\theta + m_\mathrm{b} g h \sin\theta \cos\gamma\big)\delta\sigma_1 - m_\mathrm{b} g h \sin\theta \sin\gamma\, \delta\sigma_3 \\ &+ m_\mathrm{b} g h \cos\theta \sin\gamma\, \delta\sigma_4 + M_\mathrm{b}\, \delta\sigma_5\end{aligned} \tag{44}$$

and

$$\begin{aligned}\delta P_{\text{steer}} =& \mathbf{G}_\mathrm{s} \cdot \delta \mathbf{v}_\mathrm{B} + \mathbf{M}_\mathrm{s} \cdot \delta \boldsymbol{\omega}_\mathrm{s} \\ =& \big(m_\mathrm{s} g R \sin\theta + m_\mathrm{s} g h \sin\theta \cos\gamma\big)\delta\sigma_1 - m_\mathrm{s} g h \sin\theta \sin\gamma\, \delta\sigma_3 \\ &+ m_\mathrm{s} g h \cos\theta \sin\gamma\, \delta\sigma_4 + M_\mathrm{s}\, \delta\sigma_6\,.\end{aligned} \tag{45}$$

Finally, the virtual power of the forces that act on the body has to be derived. The gravitational force acting on the body can be transformed from the F_0 frame to the F_3 frame using the rotation matrix $\mathbf{T}_{0,3}$ (cf. (1)–(3)):

$$\mathbf{G} = \begin{bmatrix} mg\cos\theta\sin\gamma \\ -mg\sin\theta \\ -mg\cos\theta\cos\gamma \end{bmatrix}_{\mathrm{F}_3}. \tag{46}$$

Note that the driving torque M_w, the balancing torque M_b, and the steering torque M_s are all internal torques. Namely, they induce reaction torques on the body with the same magnitudes but in opposite directions. Thus, the virtual power related to active forces acting on the body can be constructed as

$$\begin{aligned}\delta P_{\text{body}} =& \mathbf{G} \cdot \delta \mathbf{v}_\mathrm{B} - \big(\mathbf{M}_\mathrm{w} + \mathbf{M}_\mathrm{b} + \mathbf{M}_\mathrm{s}\big) \cdot \delta \boldsymbol{\omega} \\ =& \big(mgR\sin\theta + mgh\sin\theta\cos\gamma - M_\mathrm{b}\cos\gamma - M_\mathrm{s}\sin\gamma\big)\delta\sigma_1 \\ &+ \big(-mgh\sin\theta\sin\gamma + M_\mathrm{b}\sin\gamma - M_\mathrm{s}\cos\gamma\big)\delta\sigma_3 \\ &+ \big(mgh\cos\theta\sin\gamma - M_\mathrm{w}\big)\delta\sigma_4\,.\end{aligned} \tag{47}$$

Then, the total virtual power of the active forces is given by the sum of (41), (44), (45), and (47):

$$\delta P = \delta P_{\text{wheel}} + \delta P_{\text{body}} + \delta P_{\text{balance}} + \delta P_{\text{steer}}, \tag{48}$$

and hence, the pseudoforces Π_i can be extracted from the coefficients of the virtual pseudovelocities $\delta\sigma_i$ as

$$\begin{aligned}\Pi_1 =& \big(m_\mathrm{w} + m + m_\mathrm{b} + m_\mathrm{s}\big) g R \sin\theta + \big(m + m_\mathrm{b} + m_\mathrm{s}\big) g h \sin\theta\cos\gamma \\ &- M_\mathrm{b}\cos\gamma - M_\mathrm{s}\sin\gamma\,, \\ \Pi_2 =& M_\mathrm{w}\,, \\ \Pi_3 =& -\big(m + m_\mathrm{b} + m_\mathrm{s}\big) g h \sin\theta\sin\gamma + M_\mathrm{b}\sin\gamma - M_\mathrm{s}\cos\gamma\,, \\ \Pi_4 =& \big(m + m_\mathrm{b} + m_\mathrm{s}\big) g h \cos\theta\sin\gamma - M_\mathrm{w}\,,\end{aligned} \tag{49}$$

$$\Pi_5 = M_\mathrm{b}\,,$$
$$\Pi_6 = M_\mathrm{s}\,.$$

3.4 Equations of motion

Based on the previous subsections, the Appell equations

$$\frac{\partial S}{\partial \dot{\sigma}_i} = \Pi_i\,, \quad i = 1, \ldots, 6\,, \tag{50}$$

can be derived. These first-order differential equations depend on the pseudoaccelerations $\dot{\sigma}_i$ linearly, and thus, they can be arranged into the form:

$$\begin{aligned}
\dot{\sigma}_1 &= f_1(\sigma_1, \sigma_2, \sigma_3, \sigma_4, \sigma_5, \sigma_6, \theta, \gamma, M_\mathrm{b}, M_\mathrm{s}),\\
\dot{\sigma}_2 &= f_2(\sigma_1, \sigma_2, \sigma_3, \sigma_4, \sigma_5, \sigma_6, \theta, \gamma, M_\mathrm{w}),\\
\dot{\sigma}_3 &= f_3(\sigma_1, \sigma_2, \sigma_3, \sigma_4, \sigma_5, \sigma_6, \theta, \gamma, M_\mathrm{b}, M_\mathrm{s}),\\
\dot{\sigma}_4 &= f_4(\sigma_1, \sigma_2, \sigma_3, \sigma_4, \sigma_5, \sigma_6, \theta, \gamma, M_\mathrm{w}),\\
\dot{\sigma}_5 &= f_5(M_\mathrm{b}),\\
\dot{\sigma}_6 &= f_6(M_\mathrm{s}),
\end{aligned} \tag{51}$$

where $f_i, i = 1, \ldots, 4$ can be displayed by running the MATLAB code given in Appendix E, while f_5 and f_6 depend only on the control torques and they read

$$f_5(M_\mathrm{b}) = \frac{2M_\mathrm{b}}{m_\mathrm{b} r_\mathrm{b}^2}\,, \quad f_6(M_\mathrm{s}) = \frac{2M_\mathrm{s}}{m_\mathrm{s} r_\mathrm{s}^2}\,. \tag{52}$$

In summary, the governing equations of the system can be obtained by combining the Appell equations (51) and the kinematic equations (19). This leads to fourteen first-order differential equations, that is, the system evolves in a fourteen-dimensional state space $\sigma_1, \sigma_2, \sigma_3, \sigma_4, \sigma_5, \sigma_6, \theta, \gamma, \psi, x_\mathrm{G}, y_\mathrm{G}, \phi, \alpha, \beta$, where again the variables are ordered considering the linearization performed further below. The motion is controlled by the input torques M_w, M_b, M_s. The goal of control design is to create feedback laws that determine the torques as a function of the states so that the control objectives are achieved.

4 Control design

The model (51) and (19) constructed in the previous section can be formulated as a control affine system

$$\dot{x} = f(x) + g(x)u, \tag{53}$$

where the state vector $x \in \mathbb{R}^{14}$ and the input vector $u \in \mathbb{R}^3$ are defined as

$$x := \begin{bmatrix} \sigma_1 & \sigma_2 & \sigma_3 & \sigma_4 & \sigma_5 & \sigma_6 & \theta & \gamma & \psi & x_\mathrm{G} & y_\mathrm{G} & \phi & \alpha & \beta \end{bmatrix}^\top \tag{54}$$

and

$$u := \begin{bmatrix} M_{\mathrm{w}} & M_{\mathrm{b}} & M_{\mathrm{s}} \end{bmatrix}^{\top}, \tag{55}$$

respectively, and we have $f : \mathbb{R}^{14} \to \mathbb{R}^{14}$ and $g : \mathbb{R}^{14} \to \mathbb{R}^{3}$.

One may show that for zero input

$$u^* := \begin{bmatrix} 0 & 0 & 0 \end{bmatrix}^{\top}, \tag{56}$$

the system (53) possesses the equilibrium

$$x^* := \begin{bmatrix} 0 & \frac{v^*}{R} & 0 & 0 & \omega_{\mathrm{b}}^* & \omega_{\mathrm{s}}^* & 0 & 0 & 0 & v^* t & 0 & \frac{v^*}{R} t & \omega_{\mathrm{b}}^* t & \omega_{\mathrm{s}}^* t \end{bmatrix}^{\top}, \tag{57}$$

which corresponds to the unicycle running along the x_0-axis with constant speed v^* while the body is standing in an upright position. In this case, the constant rotational speed of the rolling wheel is $\frac{v^*}{R}$ while the constant rotational speeds ω_{b}^* and ω_{s}^* of the flywheels are considered to be nonzero for generality (cf. (17)). The control objective is set to maintain this motion.

The control objective will be achieved by establishing feedback laws of the form

$$u = k(x), \tag{58}$$

where $k : \mathbb{R}^{14} \to \mathbb{R}^{3}$. This assigns the torques in (55) as functions of the state variables in (54). Substituting (58) into (53) we obtain the closed-loop system

$$\dot{x} = f(x) + g(x)k(x), \tag{59}$$

where the right-hand side only depends on the state.

Below, we first analyze the stability of the equilibrium (57) without control and explain the self-stabilizing effect in the tilt motion. This is followed by designing a controller that can stabilize the yaw, tilt, and pitch motions simultaneously.

4.1 Open-loop dynamics

Here, we study the stability of the equilibrium by linearizing the open-loop dynamics and investigate the effects of the equilibrium speed on stability.

The linearization of the open-loop system (53) about the equilibrium (57) can be written as

$$\dot{\tilde{x}} = A\,\tilde{x} + B\,u, \tag{60}$$

where

$$A=\begin{bmatrix} 0 & 0 & A_{13} & A_{14} & 0 & 0 & A_{17} & 0 & 0 & 0 & 0 & 0 & 0 & 0 \\ A_{21} & 0 & A_{23} & 0 & 0 & 0 & 0 & A_{28} & 0 & 0 & 0 & 0 & 0 & 0 \\ A_{31} & 0 & 0 & A_{34} & 0 & 0 & 0 & 0 & 0 & 0 & 0 & 0 & 0 & 0 \\ A_{41} & 0 & A_{43} & 0 & 0 & 0 & 0 & A_{48} & 0 & 0 & 0 & 0 & 0 & 0 \\ 0 & 0 & 0 & 0 & 0 & 0 & 0 & 0 & 0 & 0 & 0 & 0 & 0 & 0 \\ 0 & 0 & 0 & 0 & 0 & 0 & 0 & 0 & 0 & 0 & 0 & 0 & 0 & 0 \\ 1 & 0 & 0 & 0 & 0 & 0 & 0 & 0 & 0 & 0 & 0 & 0 & 0 & 0 \\ 0 & 0 & 0 & 1 & 0 & 0 & 0 & 0 & 0 & 0 & 0 & 0 & 0 & 0 \\ 0 & 0 & 1 & 0 & 0 & 0 & 0 & 0 & 0 & 0 & 0 & 0 & 0 & 0 \\ 0 & R & 0 & 0 & 0 & 0 & 0 & 0 & 0 & 0 & 0 & 0 & 0 & 0 \\ -R & 0 & 0 & 0 & 0 & 0 & 0 & 0 & v^* & 0 & 0 & 0 & 0 & 0 \\ 0 & 1 & 0 & 0 & 0 & 0 & 0 & 0 & 0 & 0 & 0 & 0 & 0 & 0 \\ -1 & 0 & 0 & 0 & 1 & 0 & 0 & 0 & 0 & 0 & 0 & 0 & 0 & 0 \\ 0 & 0 & -1 & 0 & 0 & 1 & 0 & 0 & 0 & 0 & 0 & 0 & 0 & 0 \end{bmatrix},$$

$$B=\begin{bmatrix} 0 & B_{12} & 0 \\ B_{21} & 0 & 0 \\ 0 & 0 & B_{33} \\ B_{41} & 0 & 0 \\ 0 & \frac{2}{m_b r_b^2} & 0 \\ 0 & 0 & \frac{2}{m_s r_s^2} \\ 0 & 0 & 0 \\ 0 & 0 & 0 \\ 0 & 0 & 0 \\ 0 & 0 & 0 \\ 0 & 0 & 0 \\ 0 & 0 & 0 \\ 0 & 0 & 0 \\ 0 & 0 & 0 \end{bmatrix}, \tag{61}$$

and $A_{13}, A_{14}, A_{17}, A_{21}, A_{23}, A_{28}, A_{31}, A_{34}, A_{41}, A_{43}, A_{48}, B_{12}, B_{21}, B_{33}, B_{41}$ are given in Appendix B. In order to evaluate stability we compute the eigenvalues of the matrix A.

First, we discuss the case when $\omega_b^* = \omega_s^* = 0$, that is, the case when flywheels are not spinning in equilibrium (cf. (57)). Then, we have $A_{14} = A_{21} = A_{23} = A_{34} = A_{41} = A_{43} = 0$ (see Appendix B) and the eigenvalues are given by the characteristic equation

$$\det(\lambda I - A) = \left(\lambda^4 - (A_{13}A_{31} + A_{17} + A_{48})\lambda^2 + (A_{13}A_{31} + A_{17})A_{48}\right)\lambda^{10} = 0\,. \tag{62}$$

That is, the matrix A has four nonzero eigenvalues and ten zero eigenvalues. The nonzero eigenvalues can be calculated analytically as

$$\lambda_{1,2} = \pm\sqrt{A_{48}}\,, \qquad \lambda_{3,4} = \pm\sqrt{A_{13}A_{31} + A_{17}}\,, \tag{63}$$

while the corresponding eigenvectors can be found in Appendix C.

Since $A_{48} > 0$, the pair eigenvalues $\lambda_{1,2}$ are real. As one of these eigenvalues is located in the right-half complex plane, the equilibrium is unstable. The elements of the eigenvectors $v_{1,2}$ in (C1) indicate that the eigenvalue pair $\lambda_{1,2}$ is associated with the pitch dynamics of

Table 2 Parameter Values

Parameter	Value
m_{w}	2 kg
R	0.15 m
m	3 kg
h	0.3 m
m_{b}	1 kg
r_{b}	0.15 m
m_{s}	1 kg
r_{s}	0.15 m
J_x	0.1 kg m^2
J_y	0.1 kg m^2
J_z	0.02 kg m^2

the unicycle body, and that the instability corresponds to the body falling in this direction. Moreover, since $A_{13} > 0$, $A_{31} < 0$, and $A_{17} > 0$, the pair of eigenvalues $\lambda_{3,4}$ are either real or form a purely imaginary complex conjugate pair. The nonzero elements of the eigenvectors $v_{3,4}$ in (C1) indicate that the eigenvalue pair $\lambda_{3,4}$ is associated with the tilt dynamics of the unicycle.

For additional insights, the transfer functions from the input torques to the pitch, tilt, and yaw angles are calculated and included in Appendix D. It can be observed that the nonzero transfer function corresponding to the pitch angle output has its poles at $\lambda_{1,2}$. Moreover, the nonzero transfer functions corresponding to the tilt and yaw angle outputs have poles at $\lambda_{3,4}$. We also remark that among all nonzero transfer functions, only the one from steering torque to the yaw angle has nonminimum phase zeros. We will utilize these observations when designing controllers in the next section.

Using the formulas in Appendix B, one may observe that the eigenvalue pair $\lambda_{1,2}$ is independent of the speed v^*, while the speed enters the eigenvalues pair $\lambda_{3,4}$ via $A_{13}A_{31} \propto -(v^*)^2$. That is, for low speed the tilt and yaw directions are unstable, but once the velocity reaches a critical limit, i.e., $v^* > v^*_{\mathrm{cr}}$, they become (neutrally) stable. Solving the equation $A_{17} + A_{13}A_{31} = 0$, after some algebraic manipulation, we obtain the critical speed

$$v^*_{\mathrm{cr}} = \sqrt{\frac{(m_{\mathrm{w}}R^2 + m_{\mathrm{b}}r_{\mathrm{b}}^2 + 4J_z)\big(m_{\mathrm{w}}R + \widehat{m}(R+h)\big)g}{\big(3m_{\mathrm{w}}R + 2\widehat{m}(R+h)\big)m_{\mathrm{w}}R}}, \tag{64}$$

where

$$\widehat{m} = m + m_{\mathrm{b}} + m_{\mathrm{s}}. \tag{65}$$

Substituting the values in Table 2 we obtain $v^*_{\mathrm{cr}} \approx 1.51$ [m/s].

The root locus plot in Fig. 3(a) depicts how the nonzero eigenvalues (63) move in the complex plane as equilibrium speed v^* is varied between 0 and 10 [m/s]. The eigenvalue pair $\lambda_{1,2}$ stays at the same location independent of the speed. The eigenvalues of the pair $\lambda_{3,4}$ move toward each other along the real axis as v^* is increased, and after they "meet" at the origin, they become a complex conjugate pair and move away from each other along the imaginary axis. The real and imaginary parts of the eigenvalues are plotted in Fig. 3(b) and

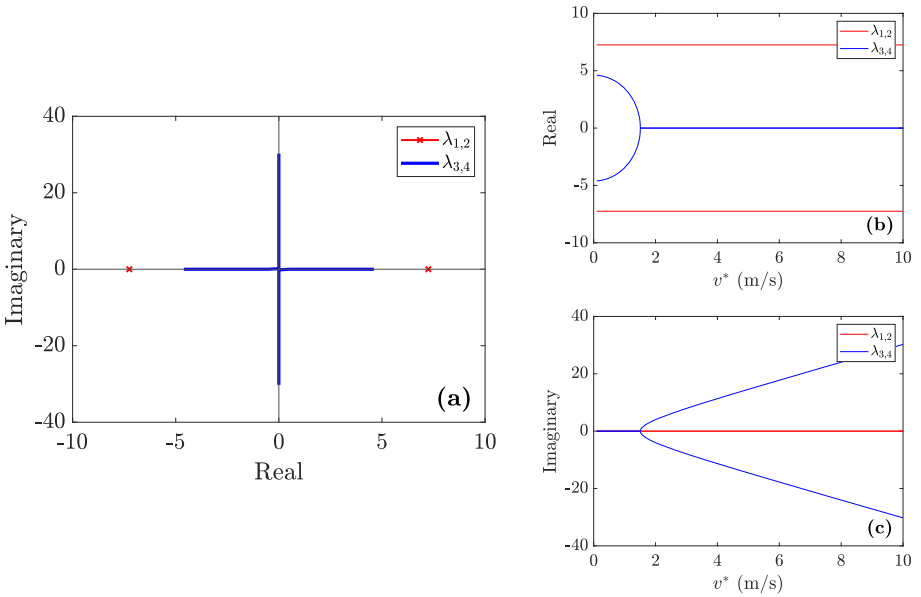

Fig. 3 (a) Root locus of nonzero eigenvalues of the linearized open-loop system when varying the speed of the rolling wheel. (b,c) Real and imaginary parts of the nonzero eigenvalues as a function of speed. The equilibrium flywheel spinning rates are $\omega_{\mathrm{b}}^* = \omega_{\mathrm{s}}^* = 0\,[\mathrm{rad/s}]$. (Color figure online)

(c), respectively. Note that the tilt is stabilized by increasing the speed despite no feedback control being applied to the system at this point. Also note that the vibration frequency increases from zero up to c. 4.8 [Hz] as the speed is increased from $v_{\mathrm{cr}}^* \approx 1.5\,[\mathrm{m/s}]$ up to $10\,[\mathrm{m/s}]$.

Such a self-stabilization effect in the tilt dynamics can also be observed in the general case when $\omega_{\mathrm{b}}^* \neq 0$ and $\omega_{\mathrm{s}}^* \neq 0$. Then, the characteristic equation becomes

$$\begin{aligned}\det(\lambda I - A) = \big(&\lambda^4 - (A_{13}A_{31} + A_{14}A_{41} + A_{34}A_{43} + A_{17} + A_{48})\lambda^2 \\ &- (A_{13}A_{34}A_{41} + A_{14}A_{31}A_{43})\lambda \\ &+ A_{13}A_{31}A_{48} + A_{17}A_{34}A_{43} + A_{17}A_{48}\big)\lambda^{10} = 0\,,\end{aligned} \tag{66}$$

cf. (62). Note that the elements A_{21}, A_{23}, and A_{28} do not appear in the characteristic equation. The matrix A still has four nonzero eigenvalues and ten zero eigenvalues. While the nonzero eigenvalues cannot be calculated analytically in this general case, the qualitative picture remains similar for moderate values of flywheel spinning rates, as illustrated in Fig. 4. The eigenvalue pair $\lambda_{1,2}$ (corresponding to the pitch dynamics) remains real, while the eigenvalue pair $\lambda_{3,4}$ (corresponding to the tilt dynamics) changes from real to complex conjugate (with a negative real part) once the equilibrium speed exceeds the critical value $v_{\mathrm{cr}}^* \approx 1.34\,[\mathrm{m/s}]$. For higher values of flywheel spinning rates, the critical speed becomes zero, that is, the eigenvalue pair $\lambda_{3,4}$ remains complex conjugate (with negative real part) in the whole range of equilibrium speed as illustrated in Fig. 5.

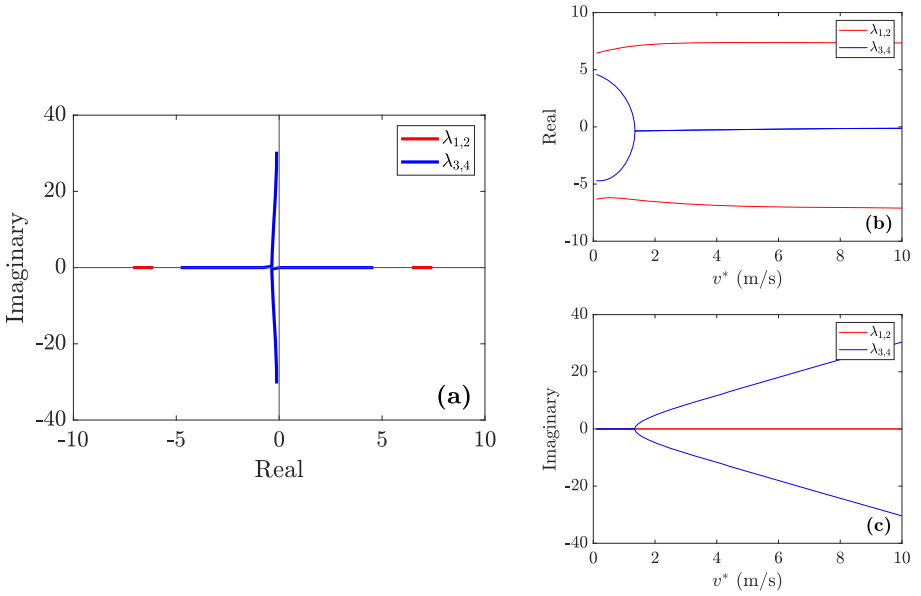

Fig. 4 (a) Root locus of nonzero eigenvalues of the linearized open-loop system when varying the speed of the rolling wheel. (b,c) Real and imaginary parts of the nonzero eigenvalues as a function of speed. The equilibrium flywheel spinning rates are $\omega_b^* = \omega_s^* = 30\,[\text{rad/s}]$. (Color figure online)

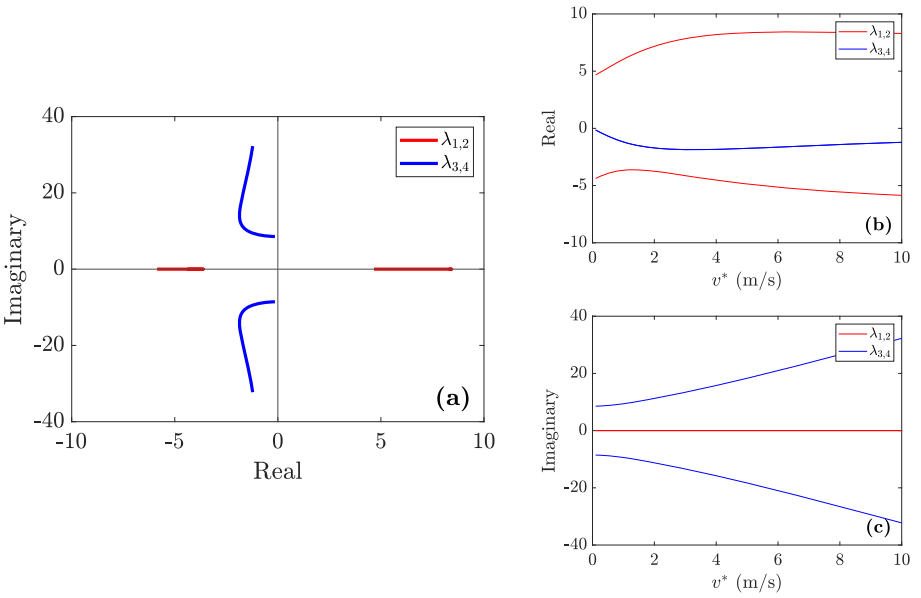

Fig. 5 (a) Root locus of nonzero eigenvalues of the linearized open-loop system when varying the speed of the rolling wheel. (b,c) Real and imaginary parts of the nonzero eigenvalues as a function of speed. The equilibrium flywheel spinning rates are $\omega_b^* = \omega_s^* = 100\,[\text{rad/s}]$. (Color figure online)

We remark that for nonzero flywheel spinning rates, the eigenvalues are not symmetric to the origin. Nevertheless, utilizing Liouville's formula [35] and that $\mathrm{tr}(A) = 0$, one may show that the nonzero eigenvalues satisfy $\sum_{j=1}^{4} \lambda_j = 0$.

4.2 Control design

The stability investigation above revealed that the pitch dynamics is unstable without control, while the tilt dynamics can be made stable (or at least neutrally stable) once the unicycle travels fast enough. From the transfer functions in Appendix D, it can be observed how the tilt, pitch, and yaw angles are affected by the three torque inputs. As a result, by constructing a feedback law one can make the pitch, the tilt, and the yaw motions asymptotically stable by moving the corresponding six eigenvalues to the left-half complex plane. This allows one to achieve the control goal of making the unicycle travel along a straight line with constant speed (cf. (57)).

For simplicity, we use proportional-derivative (PD) type control to maintain zero pitch angle γ, tilt angle θ, and yaw angle ψ:

$$\begin{aligned} M_\mathrm{w} &= p_\mathrm{w}\gamma + d_\mathrm{w}\dot{\gamma}\,, \\ M_\mathrm{b} &= p_\mathrm{b}\theta + d_\mathrm{b}\dot{\theta}\,, \\ M_\mathrm{s} &= p_\mathrm{s}\psi + d_\mathrm{s}\dot{\psi}\,. \end{aligned} \tag{67}$$

When constructing this feedback law one may consider the practical feasibility of the controller. The states used in (67) can be obtained via the use of inertial measurement units (IMU). IMUs can directly measure accelerations and angular velocity components, and by means of integration and appropriate filtering, one may obtain the yaw, tilt, and pitch angles. Alternatively, the yaw angle can be obtained directly with differential GPS or magnetic sensors.

Substituting $\dot{\theta}, \dot{\gamma}, \dot{\psi}$ from (19), the control laws can be written as functions of the state:

$$\begin{bmatrix} M_\mathrm{w} \\ M_\mathrm{b} \\ M_\mathrm{s} \end{bmatrix} = \begin{bmatrix} p_\mathrm{w}\gamma + d_\mathrm{w}(\sigma_4 - \sigma_3 \tan\theta) \\ p_\mathrm{b}\theta + d_\mathrm{b}\sigma_1 \\ p_\mathrm{s}\psi + d_\mathrm{s}\dfrac{\sigma_3}{\cos\theta} \end{bmatrix}, \tag{68}$$

cf. (54) and (55).

The control law (68) is in the form (58) and substituting this into the system (51) and (19), which fits the form (53), we obtain the closed-loop system as (59). Here, we analyze the closed-loop dynamics by linearizing (51), (19), and (68) about the equilibrium (57). This lead to

$$\dot{\tilde{x}} = \bar{A}\,\tilde{x}\,, \tag{69}$$

where

$$\bar{A} = \begin{bmatrix} \bar{A}_{11} & 0 & A_{13} & A_{14} & 0 & 0 & \bar{A}_{17} & 0 & 0 & 0 & 0 & 0 & 0 & 0 \\ A_{21} & 0 & A_{23} & \bar{A}_{24} & 0 & 0 & 0 & \bar{A}_{28} & 0 & 0 & 0 & 0 & 0 & 0 \\ A_{31} & 0 & \bar{A}_{33} & A_{34} & 0 & 0 & 0 & 0 & \bar{A}_{39} & 0 & 0 & 0 & 0 & 0 \\ A_{41} & 0 & A_{43} & \bar{A}_{44} & 0 & 0 & 0 & \bar{A}_{48} & 0 & 0 & 0 & 0 & 0 & 0 \\ \frac{2d_\mathrm{b}}{m_\mathrm{b} r_\mathrm{b}^2} & 0 & 0 & 0 & 0 & 0 & \frac{2p_\mathrm{b}}{m_\mathrm{b} r_\mathrm{b}^2} & 0 & 0 & 0 & 0 & 0 & 0 & 0 \\ 0 & 0 & \frac{2d_\mathrm{s}}{m_\mathrm{s} r_\mathrm{s}^2} & 0 & 0 & 0 & 0 & 0 & \frac{2p_\mathrm{s}}{m_\mathrm{s} r_\mathrm{s}^2} & 0 & 0 & 0 & 0 & 0 \\ 1 & 0 & 0 & 0 & 0 & 0 & 0 & 0 & 0 & 0 & 0 & 0 & 0 & 0 \\ 0 & 0 & 0 & 1 & 0 & 0 & 0 & 0 & 0 & 0 & 0 & 0 & 0 & 0 \\ 0 & 0 & 1 & 0 & 0 & 0 & 0 & 0 & 0 & 0 & 0 & 0 & 0 & 0 \\ 0 & R & 0 & 0 & 0 & 0 & 0 & 0 & 0 & 0 & 0 & 0 & 0 & 0 \\ -R & 0 & 0 & 0 & 0 & 0 & 0 & 0 & v^* & 0 & 0 & 0 & 0 & 0 \\ 0 & 1 & 0 & 0 & 0 & 0 & 0 & 0 & 0 & 0 & 0 & 0 & 0 & 0 \\ -1 & 0 & 0 & 0 & 1 & 0 & 0 & 0 & 0 & 0 & 0 & 0 & 0 & 0 \\ 0 & 0 & -1 & 0 & 0 & 1 & 0 & 0 & 0 & 0 & 0 & 0 & 0 & 0 \end{bmatrix}. \tag{70}$$

Here, the elements $A_{13}, A_{14}, A_{21}, A_{23}, A_{31}, A_{34}, A_{41}, A_{43}$ do not change compared to (61), while the elements $\bar{A}_{17}, \bar{A}_{28}, \bar{A}_{48}$ are altered by the gains $p_\mathrm{w}, d_\mathrm{w}, p_\mathrm{b}, d_\mathrm{b}, p_\mathrm{s}, d_\mathrm{s}$, and the new elements $\bar{A}_{11}, \bar{A}_{24}, \bar{A}_{33}, \bar{A}_{39}, \bar{A}_{44}$ appear for nonzero gains; see Appendix B.

One may show that the characteristic equation takes the form

$$\det(\lambda I - \bar{A}) = p(\lambda)\lambda^8 = 0\,, \tag{71}$$

where $p(\lambda)$ is a sixth-order polynomial given in Appendix B. Note that the elements A_{21}, A_{23}, $\bar{A}_{24}$, and $\bar{A}_{28}$ do not appear in the characteristic equation. The matrix $\bar{A}$ has six nonzero eigenvalues (corresponding to the pitch, tilt, and yaw motions) and eight zero eigenvalues. The pole-placement technique is used to obtain an appropriate set of control gains $p_\mathrm{w}, d_\mathrm{w}, p_\mathrm{b}, d_\mathrm{b}, p_\mathrm{s}, d_\mathrm{s}$ such that the six nonzero eigenvalues can be placed to the open left-half complex plane to achieve stability. We tuned the gains to be

$$(p_\mathrm{w}, d_\mathrm{w}, p_\mathrm{b}, d_\mathrm{b}, p_\mathrm{s}, d_\mathrm{s}) = (15, 15, 30, 15, 15, 15)\,, \tag{72}$$

which, together with the parameter choice in Table 2 and with the choice of $\omega_\mathrm{b}^* = \omega_\mathrm{s}^* = 0\,[\mathrm{rad/s}]$ and $v^* = 5\,[\mathrm{m/s}]$, yields the eigenvalues -0.35, -0.57, -0.93, -13.09, -119.97, -405.18.

We remark that, as shown by the remaining zero eigenvalues, the simple controller designed above cannot stabilize the whole dynamics. In fact, one may show that the system is not controllable at the linear level, which demands a more sophisticated nonlinear control design. Nevertheless, the designed controller enables the unicycle to travel along a straight line in a stable manner, as will be shown below by simulations.

4.3 Simulation results

Here, we use numerical simulations to illustrate the behavior of the nonlinear closed-loop system (51), (19), and (68). We test how the system responds to perturbations of different sizes around the equilibrium (57). Simulations are executed using a 4th-order Runge–Kutta method with fixed time step, to ensure small simulation errors despite the lack of damping in the system. We observed that varying time-step algorithms (that are typically built into commercial packages) failed to ensure the required accuracy.

Table 3 Initial Conditions

Set No.	1	2	3
θ_0	1°	8°	15°
γ_0	1°	8°	15°
ψ_0	1°	8°	15°

Simulations are performed using three sets of initial conditions where the angles θ, γ, and ψ are perturbed at different levels. More precisely, we use the initial condition

$$x(0) = \begin{bmatrix} 0 & \frac{v^*}{R} & 0 & 0 & 0 & 0 & \theta_0 & \gamma_0 & \psi_0 & 0 & 0 & 0 & 0 & 0 \end{bmatrix}^\top, \tag{73}$$

and the initial angles θ_0, γ_0, and ψ_0 are listed in Table 3. The parameter values are selected according to Table 2, while we use $v^* = 5\,[\mathrm{m/s}]$.

The simulation results are displayed in Fig. 6. It can be observed that when initial perturbations in θ, γ, and ψ are larger, the overshoot becomes larger and it takes a longer time for the system to settle back to the equilibrium. The required torques M_b, M_w, and M_s are also larger for larger perturbations. Nevertheless, the body is able to eventually return to the upright position and head toward the positive x_0 direction, confirming the functionality of the controller. We remark that since speed tracking is not included in the control objective, the speed $\dot{\phi} R$ settles at levels different from the initial value. Similar behavior can be observed in the rotational speeds $\dot{\alpha}$ and $\dot{\beta}$ of the balancing and steering flywheels in Fig. 7.

5 Conclusion

In this article, the dynamics of an autonomous unmanned unicycle was studied. The equations of motion were derived by using the Appellian approach that enabled us to eliminate the kinematic constraints and describe the nonholonomic dynamics using the minimal number of state variables. The acceleration energy of the multibody system as a whole was constructed and a set of nonlinear differential equations was derived. The linear stability of the upright, straight running motion was investigated and it was shown that above a critical speed, the tilt motion is stabilized even without using feedback. Then, a PD-type controller was designed that was able to stabilize the pitch, tilt, and yaw motions. It was shown by numerical simulations of the nonlinear systems that the controlled unicycle was able to balance itself and travel along a straight path while rejecting perturbations.

This work made the first step toward the creation of an autonomous unicycle. Still, there are many challenges to overcome before a working prototype can be built. Most importantly, in order to enable the unicycle to maneuver along an arbitrary path, the position variables need to be incorporated into the control design. On the one hand, this will require one to analyze the nonlinear dynamics of the system. On the other hand, the control design also needs to be performed at the nonlinear level by applying more complex nonlinear controllers. The resulting controllers need to be evaluated on higher-fidelity unicycle models that can be obtained by relaxing some of the modeling assumptions used in this work (like rolling without slipping) and/or incorporating suspension and/or tire dynamics.

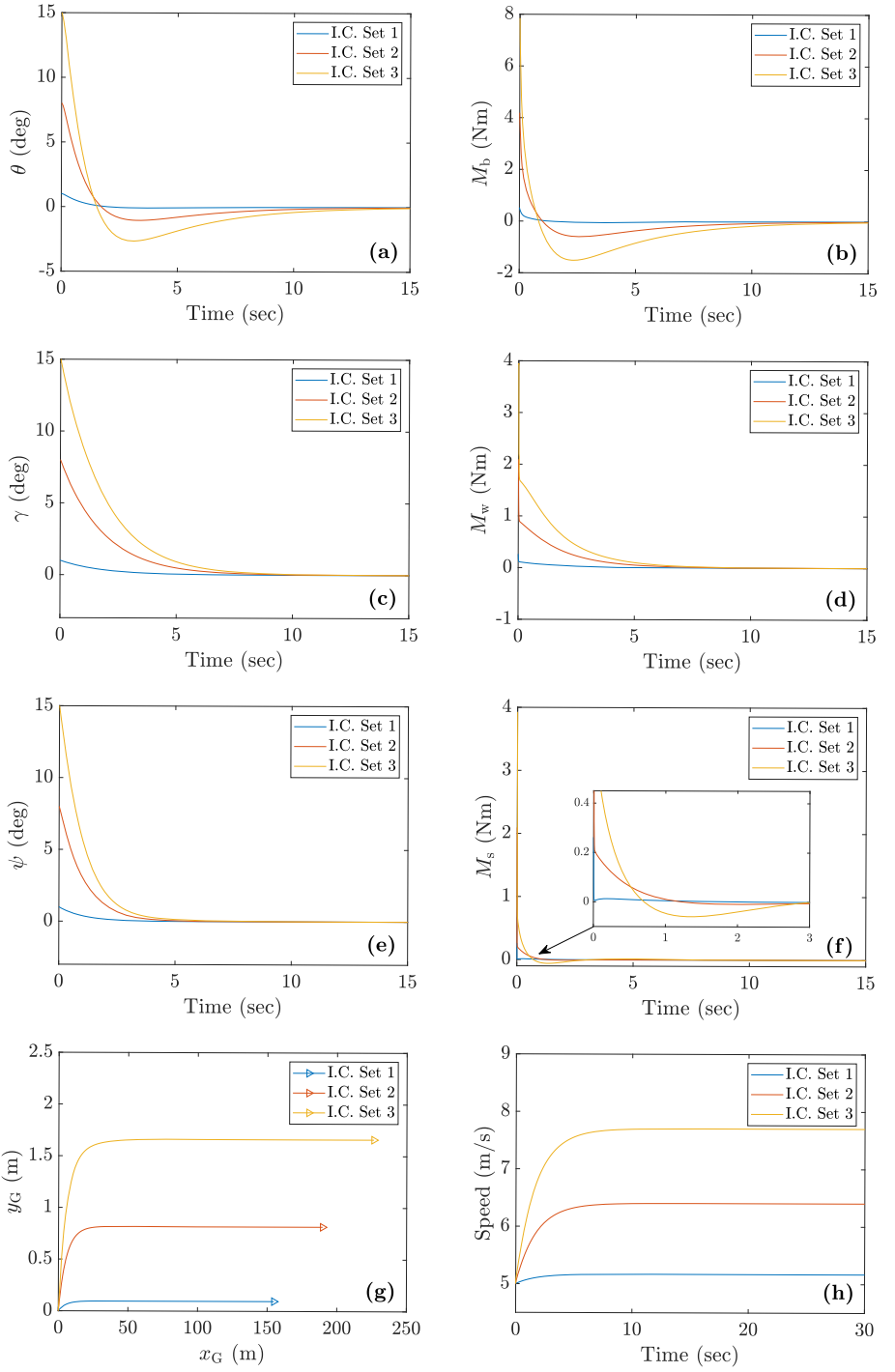

Fig. 6 Simulation results. (a–f) Time histories of the body angles and input torques. (g and h) Trajectory and speed of the center of mass G of the rolling wheel. (Color figure online)

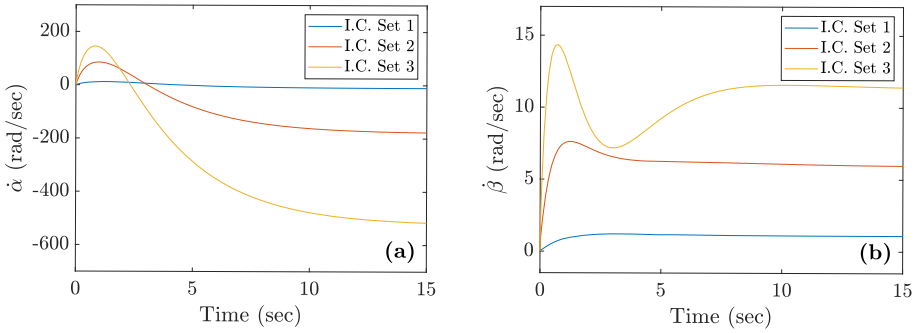

Fig. 7 Time histories of rotational speeds of (a) lateral balancing flywheel and (b) steering flywheel. (Color figure online)

Appendix A: Detailed expressions of accelerations

The components of the acceleration of the center of mass B and the angular acceleration of the body in (32) are

$$\begin{aligned} a_{\mathrm{B}x} =& \dot{\sigma}_2 R\cos\gamma + \dot{\sigma}_4 h + \sigma_1^2\big(R\sin\gamma + h\cos\gamma\sin\gamma\big) - \sigma_3^2 h\cos\gamma\sin\gamma \\ &+ \sigma_1\sigma_3\Big(R\cos\gamma + h\big(\cos^2\gamma - \sin^2\gamma\big)\Big) + \sigma_2\sigma_3 R\tan\theta\sin\gamma\,, \\ a_{\mathrm{B}y} =& -\dot{\sigma}_1(R + h\cos\gamma) + \dot{\sigma}_3 h\sin\gamma - \sigma_3^2 h\tan\theta\cos\gamma \\ &- \sigma_1\sigma_3 h\tan\theta\sin\gamma + \sigma_2\sigma_3 R + 2\sigma_1\sigma_4 h\sin\gamma + 2\sigma_3\sigma_4 h\cos\gamma\,, \\ a_{\mathrm{B}z} =& \dot{\sigma}_2 R\sin\gamma - \sigma_1^2\big(R\cos\gamma + h\cos^2\gamma\big) - \sigma_3^2 h\sin^2\gamma - \sigma_4^2 h \\ &+ \sigma_1\sigma_3\big(R\sin\gamma + 2h\cos\gamma\sin\gamma\big) - \sigma_2\sigma_3 R\tan\theta\cos\gamma \end{aligned} \tag{A1}$$

and

$$\begin{aligned} \alpha_x =& \dot{\sigma}_1\cos\gamma - \dot{\sigma}_3\sin\gamma + \sigma_3^2\tan\theta\cos\gamma \\ &+ \sigma_1\sigma_3\tan\theta\sin\gamma - \sigma_1\sigma_4\sin\gamma - \sigma_3\sigma_4\cos\gamma\,, \\ \alpha_y =& \dot{\sigma}_4\,, \\ \alpha_z =& \dot{\sigma}_1\sin\gamma + \dot{\sigma}_3\cos\gamma + \sigma_3^2\tan\theta\sin\gamma \\ &- \sigma_1\sigma_3\tan\theta\cos\gamma + \sigma_1\sigma_4\cos\gamma - \sigma_3\sigma_4\sin\gamma\,. \end{aligned} \tag{A2}$$

The components of the angular accelerations of the flywheels in (36) are

$$\begin{aligned} \alpha_{\mathrm{b}x} =& \dot{\sigma}_5\,, \\ \alpha_{\mathrm{b}y} =& \dot{\sigma}_4 - \sigma_1^2\cos\gamma\sin\gamma + \sigma_3^2\cos\gamma\sin\gamma \\ &- \sigma_1\sigma_3\big(\cos^2\gamma - \sin^2\gamma\big) + \sigma_1\sigma_5\sin\gamma + \sigma_3\sigma_5\cos\gamma\,, \\ \alpha_{\mathrm{b}z} =& \dot{\sigma}_1\sin\gamma + \dot{\sigma}_3\cos\gamma + \sigma_3^2\tan\theta\sin\gamma \\ &- \sigma_1\sigma_3\tan\theta\cos\gamma + 2\sigma_1\sigma_4\cos\gamma - 2\sigma_3\sigma_4\sin\gamma - \sigma_4\sigma_5 \end{aligned} \tag{A3}$$

and

$$\begin{aligned}\alpha_{sx} =&\dot{\sigma}_1\cos\gamma-\dot{\sigma}_3\sin\gamma+\sigma_3^2\tan\theta\cos\gamma\\&+\sigma_1\sigma_3\tan\theta\sin\gamma-2\sigma_1\sigma_4\sin\gamma-2\sigma_3\sigma_4\cos\gamma+\sigma_4\sigma_6\,,\\\alpha_{sy} =&\dot{\sigma}_4+\sigma_1^2\cos\gamma\sin\gamma-\sigma_3^2\cos\gamma\sin\gamma\\&+\sigma_1\sigma_3\big(\cos^2\gamma-\sin^2\gamma\big)-\sigma_1\sigma_6\cos\gamma+\sigma_3\sigma_6\sin\gamma\,,\\\alpha_{sz} =&\dot{\sigma}_6\,.\end{aligned}\tag{A4}$$

Appendix B: Elements of matrices in the linearized systems

The components of matrix A in (61) are:

$$\begin{aligned}&A_{13}=\frac{2\big(3m_wR+2\widehat{m}(R+h)\big)v^*}{Q_1},\quad A_{14}=-\frac{2m_sr_s^2\omega_s^*}{Q_1},\\&A_{17}=\frac{4\big(m_wR+\widehat{m}(R+h)\big)g}{Q_1},\\&A_{21}=-\frac{4\widehat{m}m_shr_s^2\omega_s^*}{RQ_2},\quad A_{23}=\frac{4\widehat{m}m_bhr_b^2\omega_b^*}{RQ_2},\quad A_{28}=-\frac{8\widehat{m}^2h^2g}{RQ_2},\\&A_{31}=-\frac{2m_wRv^*}{Q_3},\qquad A_{34}=\frac{2m_br_b^2\omega_b^*}{Q_3},\\&A_{41}=\frac{2\big(3m_w+2\widehat{m}\big)m_sr_s^2\omega_s^*}{Q_2},\quad A_{43}=-\frac{2\big(3m_w+2\widehat{m}\big)m_br_b^2\omega_b^*}{Q_2}\\&A_{48}=\frac{4\big(3m_w+2\widehat{m}\big)\widehat{m}hg}{Q_2},\end{aligned}\tag{B1}$$

the components of matrix B in (61) are:

$$\begin{aligned}&B_{12}=-\frac{4}{Q_1},\quad B_{21}=\frac{2\big(4\widehat{m}(R+h)h+m_br_b^2+m_sr_s^2+4J_y\big)}{R^2Q_2},\\&B_{33}=-\frac{4}{Q_3},\quad B_{41}=-\frac{4\big(3m_wR+2\widehat{m}(R+h)\big)}{RQ_2},\end{aligned}\tag{B2}$$

the components of matrix $\bar{A}$ in (70) are:

$$\begin{aligned}&\bar{A}_{11}=-\frac{4d_b}{Q_1},\quad \bar{A}_{17}=\frac{4\big(m_wR+\widehat{m}(R+h)\big)g-4p_b}{Q_1},\\&\bar{A}_{24}=\frac{2\big(4\widehat{m}(R+h)h+m_br_b^2+m_sr_s^2+4J_y\big)d_w}{R^2Q_2},\\&\bar{A}_{28}=-\frac{8\widehat{m}^2Rh^2g-2\big(4\widehat{m}(R+h)h+m_br_b^2+m_sr_s^2+4J_y\big)p_w}{R^2Q_2},\\&\bar{A}_{33}=-\frac{4d_s}{Q_3},\quad \bar{A}_{39}=-\frac{4p_s}{Q_3},\end{aligned}\tag{B3}$$

$$\bar{A}_{44} = -\frac{4\big(3m_{\mathrm{w}}R + 2\widehat{m}(R+h)\big)d_{\mathrm{w}}}{RQ_2},$$
$$\bar{A}_{48} = \frac{4\widehat{m}\big(3m_{\mathrm{w}} + 2\widehat{m}\big)Rhg - 4\big(3m_{\mathrm{w}}R + 2\widehat{m}(R+h)\big)p_{\mathrm{w}}}{RQ_2},$$

where

$$\begin{aligned}
\widehat{m} =& m + m_{\mathrm{b}} + m_{\mathrm{s}},\\
Q_1 =& 5m_{\mathrm{w}}R^2 + 4\widehat{m}(R+h)^2 + m_{\mathrm{s}}r_{\mathrm{s}}^2 + 4J_x,\\
Q_2 =& \big(3m_{\mathrm{w}} + 2\widehat{m}\big)\big(m_{\mathrm{b}}r_{\mathrm{b}}^2 + m_{\mathrm{s}}r_{\mathrm{s}}^2 + 4J_y\big) + 12\widehat{m}m_{\mathrm{w}}h^2,\\
Q_3 =& m_{\mathrm{w}}R^2 + m_{\mathrm{b}}r_{\mathrm{b}}^2 + 4J_z.
\end{aligned} \tag{B4}$$

The polynomial in (71) is:

$$\begin{aligned}
p(\lambda) = \lambda^6 &- (\bar{A}_{11} + \bar{A}_{33} + \bar{A}_{44})\lambda^5 + (\bar{A}_{11}\bar{A}_{33} + \bar{A}_{11}\bar{A}_{44} - A_{13}A_{31} - A_{14}A_{41}\\
&+ \bar{A}_{33}\bar{A}_{44} - A_{34}A_{43} - \bar{A}_{17} - \bar{A}_{39} - \bar{A}_{48})\lambda^4\\
&+ (-\bar{A}_{11}\bar{A}_{33}\bar{A}_{44} + \bar{A}_{11}A_{34}A_{43} + A_{13}A_{31}\bar{A}_{44} - A_{13}A_{34}A_{41}\\
&- A_{14}A_{31}A_{43} + A_{14}\bar{A}_{33}A_{41} + \bar{A}_{11}\bar{A}_{39} + \bar{A}_{11}\bar{A}_{48} + \bar{A}_{17}\bar{A}_{33}\\
&+ \bar{A}_{17}\bar{A}_{44} + \bar{A}_{33}\bar{A}_{48} + \bar{A}_{39}\bar{A}_{44})\lambda^3 + (-\bar{A}_{11}\bar{A}_{33}\bar{A}_{48} - \bar{A}_{11}\bar{A}_{39}\bar{A}_{44} + A_{13}A_{31}\bar{A}_{48}\\
&+ A_{14}\bar{A}_{39}A_{41} - \bar{A}_{17}\bar{A}_{33}\bar{A}_{44} + \bar{A}_{17}A_{34}A_{43} + \bar{A}_{17}\bar{A}_{39} + \bar{A}_{17}\bar{A}_{48} + \bar{A}_{39}\bar{A}_{48})\lambda^2\\
&- (\bar{A}_{11}\bar{A}_{39}\bar{A}_{48} + \bar{A}_{17}\bar{A}_{33}\bar{A}_{48} + \bar{A}_{17}\bar{A}_{39}\bar{A}_{44})\lambda - \bar{A}_{17}\bar{A}_{39}\bar{A}_{48}\,.
\end{aligned} \tag{B5}$$

Appendix C: Eigenvectors of the open-loop system

When $\omega_{\mathrm{b}}^* = \omega_{\mathrm{s}}^* = 0$, the eigenvectors corresponding to the nonzero eigenvalues (63) are

$$v_{1,2} = \begin{bmatrix} 0\\ \pm\sqrt{A_{48}}\\ 0\\ \frac{\pm(\sqrt{A_{48}})^3}{A_{28}}\\ 0\\ 0\\ 0\\ \frac{A_{48}}{A_{28}}\\ 0\\ R\\ 0\\ 1\\ 0\\ 0 \end{bmatrix}, \quad v_{3,4} = \begin{bmatrix} -\frac{A_{13}A_{31}+A_{17}}{A_{31}}\\ 0\\ \mp\sqrt{A_{13}A_{31}+A_{17}}\\ 0\\ 0\\ 0\\ \frac{\mp\sqrt{A_{13}A_{31}+A_{17}}}{A_{31}}\\ 0\\ -1\\ 0\\ \pm\big(\frac{R\sqrt{A_{13}A_{31}+A_{17}}}{A_{31}} - \frac{v^*}{\sqrt{A_{13}A_{31}+A_{17}}}\big)\\ 0\\ \frac{\pm\sqrt{A_{13}A_{31}+A_{17}}}{A_{31}}\\ 1 \end{bmatrix}, \tag{C1}$$

where A_{ij}, B_{ij} are defined in Appendix B.

Appendix D: Transfer functions for the open-loop system

When $\omega_b^* = \omega_s^* = 0$, the transfer function from input torques M_w, M_b, and M_s to angles γ, θ, and ψ are:

$$
\begin{aligned}
T_{M_w\to\gamma}(\lambda) &= \frac{B_{41}}{\lambda^2 - A_{48}}\,,\\
T_{M_b\to\theta}(\lambda) &= \frac{B_{12}}{\lambda^2 - (A_{13}A_{31} + A_{17})}\,,\\
T_{M_s\to\psi}(\lambda) &= \frac{B_{33}(\lambda^2 - A_{17})}{\lambda^2\big(\lambda^2 - (A_{13}A_{31} + A_{17})\big)}\,,\\
T_{M_b\to\psi}(\lambda) &= \frac{A_{31}B_{12}}{\lambda\big(\lambda^2 - (A_{13}A_{31} + A_{17})\big)}\,,\\
T_{M_s\to\theta}(\lambda) &= \frac{A_{13}B_{33}}{\lambda\big(\lambda^2 - (A_{13}A_{31} + A_{17})\big)}\,,\\
T_{M_w\to\theta}(\lambda) &= T_{M_b\to\gamma}(\lambda) = T_{M_s\to\gamma}(\lambda) = T_{M_w\to\psi}(\lambda) = 0\,,
\end{aligned}
\tag{D1}
$$

where A_{ij}, B_{ij} can be found in Appendix B.

Appendix E: MATLAB code for the EoM derivation

```
%% Define Parameter Symbols
syms m_w R m h J_x J_y J_z m_b r_b m_s r_s g M_w M_b M_s delta...
    x_G y_G z_G psi theta phi gamma alpha beta x_dot_G y_dot_G z_dot_G...
    psi_dot theta_dot phi_dot gamma_dot alpha_dot beta_dot...
    sigma1 sigma2 sigma3 sigma4 sigma5 sigma6...
    sigma_dot_1 sigma_dot_2 sigma_dot_3 sigma_dot_4 sigma_dot_5 sigma_dot_6;

%% Frame Transformation
T_02=[cos(psi),sin(psi),0;...
    -cos(theta)*sin(psi),cos(psi)*cos(theta),sin(theta);...
    sin(psi)*sin(theta),-cos(psi)*sin(theta),cos(theta)];
T_23=[cos(gamma),0,-sin(gamma);...
    0,1,0;...
    sin(gamma),0,cos(gamma)];
T_03=T_23*T_02;

%% Constraints Derivation
vG_F0=[x_dot_G;y_dot_G;z_dot_G];
omega_w_F2=T_02*[0;0;psi_dot]+[theta_dot;phi_dot;0];
rGP_F2=[0;0;-R];
vP_F0=vG_F0+inv(T_02)*cross(omega_w_F2,rGP_F2);
vP_F0=simplify(vP_F0);
constraints=vP_F0==[0;0;0];
% kinematic constraints
KC=[vP_F0(1);vP_F0(2)]==[0;0];
% geometric constaints
GC=z_G==R*cos(theta);
```

```
%% Pseudo Velocities
omega_F3=T_03*[0;0;psi_dot]+T_23*[theta_dot;0;0]+[0;gamma_dot;0];
omega_b_F3=omega_F3+[alpha_dot;0;0];
omega_s_F3=omega_F3+[0;0;beta_dot];
% pseudo velocities
pseudo_vel=[sigma1;sigma2;sigma3;sigma4;sigma5;sigma6]==...
    [omega_w_F2;omega_F3(2);omega_b_F3(1);omega_s_F3(3)];

%% Kinematics Equations
A=[1,0,-R*cos(psi)*sin(theta),-R*cos(theta)*sin(psi),-R*cos(psi),0,0,0;...
    0,1,-R*sin(psi)*sin(theta),R*cos(psi)*cos(theta),-R*sin(psi),0,0,0;...
    0,0,0,1,0,0,0,0;...
    0,0,sin(theta),0,1,0,0,0;...
    0,0,cos(theta),0,0,0,0,0;...
    0,0,sin(theta),0,0,1,0,0;...
    0,0,-cos(theta)*sin(gamma),cos(gamma),0,0,1,0;...
    0,0,cos(gamma)*cos(theta),sin(gamma),0,0,0,1];
det(A);
B=[x_dot_G;y_dot_G;psi_dot;theta_dot;phi_dot;gamma_dot;alpha_dot;beta_dot];
C=[0;0;sigma1;sigma2;sigma3;sigma4;sigma5;sigma6];
A*B==C;
B_soln=inv(A)*C;
% kinematic equations
EOM_p1=B==B_soln;

%% Acceleration Energy of Wheel
vG_F2=[0;0;0]-cross(omega_w_F2,rGP_F2);
vG_F2=subs(vG_F2,B,B_soln);
omega_20_F2=T_02*[0;0;psi_dot]+[theta_dot;0;0];
omega_20_F2=subs(omega_20_F2,B,B_soln);
aG_F2=[R*sigma_dot_2;-R*sigma_dot_1;0]+cross(omega_20_F2,vG_F2);
S_wheel_T1=(1/2)*m_w*(aG_F2(1)^2+aG_F2(2)^2+aG_F2(3)^2);

omega_w_F2=[sigma1;sigma2;sigma3];
alpha_w_F2=[sigma_dot_1;sigma_dot_2;sigma_dot_3]...
    +cross(omega_20_F2,omega_w_F2);
J_w_F2=[(1/4)*m_w*R^2,0,0;...
    0,(1/2)*m_w*R^2,0;...
    0,0,(1/4)*m_w*R^2];
S_wheel_T2=(1/2)*[alpha_w_F2(1),alpha_w_F2(2),alpha_w_F2(3)]...
    *J_w_F2*alpha_w_F2;

H_w_F2=J_w_F2*omega_w_F2;
S_wheel_T3=det([alpha_w_F2(1),alpha_w_F2(2),alpha_w_F2(3);...
    omega_w_F2(1),omega_w_F2(2),omega_w_F2(3);...
    H_w_F2(1),H_w_F2(2),H_w_F2(3)]);

S_wheel=S_wheel_T1+S_wheel_T2+S_wheel_T3;

%% Acceleration Energy of Body
vG_F3=T_23*vG_F2;
omega_F3=subs(omega_F3,B,B_soln);
rGB_F3=[0;0;h];
vB_F3=vG_F3+cross(omega_F3,rGB_F3);
vB_F3_local_der(1,1)=h*sigma_dot_4+R*(sigma_dot_2*cos(gamma)...
    -sigma2*gamma_dot*sin(gamma));
vB_F3_local_der(2,1)=-R*sigma_dot_1-h*(sigma_dot_1*cos(gamma)...
    -sigma1*gamma_dot*sin(gamma)-sigma_dot_3*sin(gamma)...
    -sigma3*gamma_dot*cos(gamma));
vB_F3_local_der(3,1)=R*(sigma_dot_2*sin(gamma)+sigma2*gamma_dot*cos(gamma));
vB_F3_local_der=subs(vB_F3_local_der,B,B_soln);
omega_30_F3=omega_F3;
aB_F3=vB_F3_local_der+cross(omega_30_F3,vB_F3);
S_body_T1=(1/2)*m*(aB_F3(1)^2+aB_F3(2)^2+aB_F3(3)^2);

omega_F3_local_der(1,1)=sigma_dot_1*cos(gamma)-sigma1*gamma_dot*sin(gamma)...
    -sigma_dot_3*sin(gamma)-sigma3*gamma_dot*cos(gamma);
```

```
omega_F3_local_der(2,1)=sigma_dot_4;
omega_F3_local_der(3,1)=sigma_dot_3*cos(gamma)-sigma3*gamma_dot*sin(gamma)...
    +sigma_dot_1*sin(gamma)+sigma1*gamma_dot*cos(gamma);
omega_F3_local_der=subs(omega_F3_local_der,B,B_soln);
alpha_F3=omega_F3_local_der+cross(omega_30_F3,omega_F3);
J_F3=[J_x,0,0;0,J_y,0;0,0,J_z];
S_body_T2=(1/2)*[alpha_F3(1),alpha_F3(2),alpha_F3(3)]*J_F3*alpha_F3;

H_F3=J_F3*omega_F3;
S_body_T3=det([alpha_F3(1),alpha_F3(2),alpha_F3(3);...
    omega_F3(1),omega_F3(2),omega_F3(3);...
    H_F3(1),H_F3(2),H_F3(3)]);

S_body=S_body_T1+S_body_T2+S_body_T3;

%% Acceleration Energy of Balancing Flywheel
S_balance_T1=(1/2)*m_b*(aB_F3(1)^2+aB_F3(2)^2+aB_F3(3)^2);

omega_b_F3=subs(omega_b_F3,B,B_soln);
omega_b_F3_local_der(1,1)=sigma_dot_5;
omega_b_F3_local_der(2,1)=sigma_dot_4;
omega_b_F3_local_der(3,1)=sigma_dot_3*cos(gamma)...
    -sigma3*gamma_dot*sin(gamma)+sigma_dot_1*sin(gamma)...
    +sigma1*gamma_dot*cos(gamma);
omega_b_F3_local_der=subs(omega_b_F3_local_der,B,B_soln);
alpha_b_F3=omega_b_F3_local_der+cross(omega_30_F3,omega_b_F3);
J_b_F3=[(1/2)*m_b*r_b^2,0,0;0,(1/4)*m_b*r_b^2,0;0,0,(1/4)*m_b*r_b^2];
S_balance_T2=(1/2)*[alpha_b_F3(1),alpha_b_F3(2),alpha_b_F3(3)]...
    *J_b_F3*alpha_b_F3;

H_b_F3=J_b_F3*omega_b_F3;
S_balance_T3=det([alpha_b_F3(1),alpha_b_F3(2),alpha_b_F3(3);...
    omega_b_F3(1),omega_b_F3(2),omega_b_F3(3);...
    H_b_F3(1),H_b_F3(2),H_b_F3(3)]);

S_balance=S_balance_T1+S_balance_T2+S_balance_T3;

%% Acceleration Energy of Steering Flywheel
S_steer_T1=(1/2)*m_s*(aB_F3(1)^2+aB_F3(2)^2+aB_F3(3)^2);

omega_s_F3=subs(omega_s_F3,B,B_soln);
omega_s_F3_local_der(1,1)=sigma_dot_1*cos(gamma)...
    -sigma1*gamma_dot*sin(gamma)-sigma_dot_3*sin(gamma)...
    -sigma3*gamma_dot*cos(gamma);
omega_s_F3_local_der(2,1)=sigma_dot_4;
omega_s_F3_local_der(3,1)=sigma_dot_6;
omega_s_F3_local_der=subs(omega_s_F3_local_der,B,B_soln);
alpha_s_F3=omega_s_F3_local_der+cross(omega_30_F3,omega_s_F3);
J_s_F3=[(1/4)*m_s*r_s^2,0,0;0,(1/4)*m_s*r_s^2,0;0,0,(1/2)*m_s*r_s^2];
S_steer_T2=(1/2)*[alpha_s_F3(1),alpha_s_F3(2),alpha_s_F3(3)]...
    *J_s_F3*alpha_s_F3;

H_s_F3=J_s_F3*omega_s_F3;
S_steer_T3=det([alpha_s_F3(1),alpha_s_F3(2),alpha_s_F3(3);...
    omega_s_F3(1),omega_s_F3(2),omega_s_F3(3);...
    H_s_F3(1),H_s_F3(2),H_s_F3(3)]);

S_steer=S_steer_T1+S_steer_T2+S_steer_T3;

%% Total Acceleration Energy
S=S_wheel+S_body+S_balance+S_steer;

%% Virtual Power
% virtual power of rolling wheel
G_w_F2=T_02*[0;0;-m_w*g];
M_w_F2=[0;M_w;0];
M_w_F3=T_23*M_w_F2;
delta_P_wheel=[G_w_F2(1),G_w_F2(2),G_w_F2(3)]...
```

```
    *[delta*vG_F2(1);delta*vG_F2(2);delta*vG_F2(3)]+...
    [M_w_F2(1),M_w_F2(2),M_w_F2(3)]...
    *[delta*omega_w_F2(1);delta*omega_w_F2(2);delta*omega_w_F2(3)];

% virtual power of balancing flywheel
G_b_F3=T_03*[0;0;-m_b*g];
M_b_F3=[M_b;0;0];
delta_P_balance=[G_b_F3(1),G_b_F3(2),G_b_F3(3)]...
    *[delta*vB_F3(1);delta*vB_F3(2);delta*vB_F3(3)]+...
    [M_b_F3(1),M_b_F3(2),M_b_F3(3)]...
    *[delta*omega_b_F3(1);delta*omega_b_F3(2);delta*omega_b_F3(3)];

% virtual power of steering flywheel
G_s_F3=T_03*[0;0;-m_s*g];
M_s_F3=[0;0;M_s];
delta_P_steer=[G_s_F3(1),G_s_F3(2),G_s_F3(3)]...
    *[delta*vB_F3(1);delta*vB_F3(2);delta*vB_F3(3)]+...
    [M_s_F3(1),M_s_F3(2),M_s_F3(3)]...
    *[delta*omega_s_F3(1);delta*omega_s_F3(2);delta*omega_s_F3(3)];

% virtual power of body
G_F3=T_03*[0;0;-m*g];
delta_P_body=[G_F3(1),G_F3(2),G_F3(3)]...
    *[delta*vB_F3(1);delta*vB_F3(2);delta*vB_F3(3)]+...
    [-M_w_F3(1),-M_w_F3(2),-M_w_F3(3)]...
    *[delta*omega_F3(1);delta*omega_F3(2);delta*omega_F3(3)]+...
    [-M_b_F3(1),-M_b_F3(2),-M_b_F3(3)]...
    *[delta*omega_F3(1);delta*omega_F3(2);delta*omega_F3(3)]+...
    [-M_s_F3(1),-M_s_F3(2),-M_s_F3(3)]...
    *[delta*omega_F3(1);delta*omega_F3(2);delta*omega_F3(3)];

% total virtual power
delta_P=delta_P_wheel+delta_P_balance+delta_P_steer+delta_P_body;

%% Pseudo forces
Pi_1=R*g*(m+m_w+m_b+m_s)*sin(theta)...
    +g*h*(m+m_b+m_s)*cos(gamma)*sin(theta)-M_b*cos(gamma)-M_s*sin(gamma);
Pi_2=M_w;
Pi_3=M_b*sin(gamma)-M_s*cos(gamma)-g*h*(m+m_b+m_s)*sin(gamma)*sin(theta);
Pi_4=g*h*(m+m_b+m_s)*cos(theta)*sin(gamma)-M_w;
Pi_5=M_b;
Pi_6=M_s;

%% Appell Equations
Appell_1=simplify(diff(S,sigma_dot_1))==Pi_1;
Appell_2=simplify(diff(S,sigma_dot_2))==Pi_2;
Appell_3=simplify(diff(S,sigma_dot_3))==Pi_3;
Appell_4=simplify(diff(S,sigma_dot_4))==Pi_4;
Appell_5=simplify(diff(S,sigma_dot_5))==Pi_5;
Appell_6=simplify(diff(S,sigma_dot_6))==Pi_6;

[sigma_dot_1_soln,sigma_dot_2_soln,sigma_dot_3_soln,...
    sigma_dot_4_soln,sigma_dot_5_soln,sigma_dot_6_soln]=...
    solve([Appell_1,Appell_2,Appell_3,Appell_4,Appell_5,Appell_6],...
    [sigma_dot_1,sigma_dot_2,sigma_dot_3,sigma_dot_4,sigma_dot_5,sigma_dot_6]);

%% EOM
% Appell equations
EOM_p2=...
    [sigma_dot_1==simplify(expand(sigma_dot_1_soln),'Steps',50);... % f_1
    sigma_dot_2==simplify(expand(sigma_dot_2_soln),'Steps',50);...  % f_2
    sigma_dot_3==simplify(expand(sigma_dot_3_soln),'Steps',50);...  % f_3
    sigma_dot_4==simplify(expand(sigma_dot_4_soln),'Steps',50);...  % f_4
    sigma_dot_5==simplify(expand(sigma_dot_5_soln),'Steps',50);...  % f_5
    sigma_dot_6==simplify(expand(sigma_dot_6_soln),'Steps',50)];    % f_6

% EOM
EOM=[EOM_p2;EOM_p1];
```

Author contributions X. C. and D. C. B. carried out the analytical calculations as well as the numerical simulations. They contributed equally to this work. D. T. created some of the illustrations. D. T. and G. O. supervised the research and all authors participated in the writing of the manuscript.

Funding Dénes Takács acknowledges the support of the Rosztoczy Foundation during 2020–2021. Dang Cong Bui acknowledges the support of the Vingroup Science and Technology Scholarship Program during 2021–2022. Gábor Orosz acknowledges the support of Hungarian Academy of Sciences within the Distinguished Guest Fellowship Programme during 2022.

Code Availability The codes used to generate the data are included in the appendix.

Declarations

Ethical Approval Not applicable.

Competing interests The authors declare no competing interests.

References

1. Appell, P.: Sur une forme générale des équations de la dynamique (On a general form of the equations of dynamics). J. Reine Angew. Math. **121**, 310–319 (1900)
2. Baruh, H.: Analytical Dynamics. McGraw-Hill, New York (1999)
3. Bloch, A.M.: Nonholonomic Mechanics and Control. Springer, Berlin (2003)
4. De Luca, A., Oriolo, G., Samson, C.: Feedback control of a nonholonomic car-like robot. In: Laumond, J.P. (ed.) Robot Motion Planning and Control, pp. 171–249. Springer, Berlin (1998)
5. De Sapio, V.: Advanced Analytical Dynamics: Theory and Applications. Cambridge University Press, Cambridge (2017)
6. Desloge, E.: A comparison of Kane's equations of motion and the Gibbs–Appell equations of motion. Am. J. Phys. **54**, 470–472 (1986)
7. Desloge, E.: Relationship between Kane's equations and the Gibbs-Appell equations. J. Guid. Control Dyn. **10**, 120–1222 (1987)
8. Desloge, E.: The Gibbs-Appell equations of motion. Am. J. Phys. **56**, 841–846 (1988)
9. Gantmacher, F.: Lectures in Analytical Mechanics. MIR Publishers, Moscow (1970)
10. Gibbs, J.W.: On the fundamental formulae of dynamics. Am. J. Math. **2**(1), 49–64 (1879)
11. Greenwood, D.T.: Adavanced Dynamics. Cambridge University Press, Cambridge (2003)
12. Halvani, O., Or, Y.: Nonholonomic dynamics of the twistcar vehicle: asymptotic analysis and hybrid dynamics of frictional skidding. Nonlinear Dyn. **107**(3), 3443–3459 (2022)
13. Hamel, G.: Nichtholonome Systeme höherer Art (Nonholonomic systems of a higher kind). Sitzungsber. Berl. Math. Ges. **37**, 41–52 (1938)
14. Horvath, H.Z., Takács, D.: Control design for balancing a motorbike at zero longitudinal speed. In: 15th International Symposium on Advanced Vehicle Control (2022)
15. Isomi, Y., Majima, S.: Tracking control method for an underactuated unicycle robot using an equilibrium state. In: 2009 IEEE International Conference on Control and Automation, pp. 1844–1849 (2009)
16. Kane, T.R.: Dynamics of nonholonomic systems. J. Appl. Mech. **28**, 574–578 (1961)
17. Kane, T.: Rebuttal to "A comparison of Kane's equations of motion and the Gibbs–Appell equations of motion". Am. J. Phys. **54**, 472 (1986)
18. Kane, T.R., Levinson, D.A.: Dynamics, Theory and Applications. McGraw-Hill, New York (1985)
19. Koon, W.S., Marsden, J.E.: The Hamiltonian and Lagrangian approaches to the dynamics of nonholonomic systems. Rep. Math. Phys. **40**(1), 21–62 (1997)
20. Meijaard, J.P., Papadopoulos, J.M., Ruina, A., et al.: Linearized dynamics equations for the balance and steer of a bicycle: a benchmark and review. Proc. R. Soc. A **463**(2084), 1955–1982 (2007)
21. Naveh, Y., Bar Yoseph, P., Halevi, Y.: Nonlinear modeling and control of a unicycle. Dyn. Control **9**, 279–296 (1999)
22. Neimark, J.I., Fufaev, N.A.: Dynamics of Nonholonomic Systems. Translations of Mathematical Monographs, vol. 33. Am. Math. Soc., Providence (1972)
23. Niełaczny, M., Wiesław, B., Kapitaniak, T.: Dynamics of the Unicycle Modelling and Experimental Verification. Springer, Berlin (2019)

24. Ostrovskaya, S., Angeles, J.: Nonholonomic systems revisited within the framework of analytical mechanics. Appl. Mech. Rev. **57**(7), 415–433 (1998)
25. Papastavridis, J.G.: Analytical Mechanics. World Scientific, Singapore (2002)
26. Pollard, B., Fedonyuk, V., Tallapragada, P.: Swimming on limit cycles with nonholonomic constraints. Nonlinear Dyn. **97**(4), 2453–2468 (2019)
27. Qin, W.B., Zhang, Y., Takács, D., et al.: Nonholonomic dynamics and control of road vehicles: moving toward automation. Nonlinear Dyn. **110**(3), 1959–2004 (2022)
28. Rodwell, C., Tallapragada, P.: Induced and tunable multistability due to nonholonomic constraints. Nonlinear Dyn. **108**(3), 2115–2126 (2022)
29. Routh, E.J.: The Advanced Part of a Treatise on the Dynamics of a System of Rigid Bodies. Macmillan & Co., London (1884)
30. Ruan, X., Hu, J., Wang, Q.: Modeling with Euler-Lagrange equation and cybernetical analysis for a unicycle robot. In: 2nd International Conference on Intelligent Computation Technology and Automation, pp. 108–111 (2009)
31. Schoonwinkel, A.: Design and test of a computer stabilized unicycle. PhD thesis, Stanford University (1987)
32. Sheng, Z., Yamafuji, K.: Study on the stability and motion control of a unicycle: part I: dynamics of a human riding a unicycle and its modeling by link mechanisms. JSME Int. J. Ser. C **38**(2), 249–259 (1995)
33. Suzuki, H., Moromugi, S., Okura, T.: Development of robotic unicycles. J. Robot. Mechatron. **26**(5), 540–549 (2014)
34. Tallapragada, P., Kelly, S.D.: Integrability of velocity constraints modeling vortex shedding in ideal fluids. J. Comput. Nonlinear Dyn. **021**, 008 (2017)
35. Teschl, G.: Ordinary Differential Equations and Dynamical System. Am. Math. Soc., Providence (2012)
36. Várszegi, B., Takács, D., Orosz, G.: On the nonlinear dynamics of automated vehicles – a nonholonomic approach. Eur. J. Mech. A, Solids **74**, 371–380 (2019)
37. Voronets, P.V.: Об уравнениях движения для неголономных систем (On the equations of motion of nonholonomic systems). Мат. Сб. **22**(4), 659–686 (1901)
38. Vos, D., Von Flotow, A.: Dynamics and nonlinear adaptive control of an autonomous unicycle: theory and experiment. In: 29th IEEE Conference on Decision and Control, pp. 182–187 (1990)
39. Voss, A.: Ueber die Differentialgleichungen der Mechanik (About the differential equations of mechanics). Math. Ann. **25**, 258–286 (1885)
40. Yona, T., Or, Y.: The wheeled three-link snake model: singularities in nonholonomic constraints and stick-slip hybrid dynamics induced by Coulomb friction. Nonlinear Dyn. **95**(3), 2307–2324 (2019)
41. Zenkov, D., Bloch, A., Marsden, J.: The Lyapunov-Malkin theorem and stabilization of the unicycle with rider. Syst. Control Lett. **45**, 293–300 (2002)